Time-dependent density functional study of the electronic spectra of oligoacenes in the charge states −1, 0, +1, and +2

ARTICLE *in* CHEMICAL PHYSICS · NOVEMBER 2007

Impact Factor: 1.65 · DOI: 10.1016/j.chemphys.2007.07.046 · Source: arXiv

4 AUTHORS, INCLUDING:

Giuliano Malloci
Italian National Research Council
62 PUBLICATIONS **756** CITATIONS
SEE PROFILE

Giacomo Mulas
National Institute of Astrophysics
85 PUBLICATIONS **941** CITATIONS
SEE PROFILE

G. Cappellini
Università degli studi di Cagliari
78 PUBLICATIONS **958** CITATIONS
SEE PROFILE

Available online at www.sciencedirect.com
ScienceDirect
Chemical Physics 340 (2007) 43–58
Chemical Physics
www.elsevier.com/locate/chemphys

Time-dependent density functional study of the electronic spectra of oligoacenes in the charge states −1, 0, +1, and +2

G. Malloci [a,*], G. Mulas [a], G. Cappellini [b,a], C. Joblin [c]

[a] *INAF – Osservatorio Astronomico di Cagliari–Astrochemistry Group, Strada 54, Località Poggio dei Pini, I-09012 Capoterra (CA), Italy*
[b] *CNR – Sardinian Laboratory for Computational Materials Science, CNISM and Dipartimento di Fisica, Università degli Studi di Cagliari, Cittadella Universitaria, Strada Prov. le Monserrato-Sestu Km 0.700, I-09042 Monserrato (CA), Italy*
[c] *Centre d'Etude Spatiale des Rayonnements, Université Toulouse 3, CNRS, Observatoire Midi-Pyrénées, 9 Avenue du Colonel Roche, 31028 Toulouse Cedex 4, France*

Received 23 February 2007; accepted 20 July 2007
Available online 9 August 2007

Abstract

We present a systematic theoretical study of the five smallest oligoacenes (naphthalene, anthracene, tetracene, pentacene, and hexacene) in their anionic, neutral, cationic, and dicationic charge states. We used density functional theory (DFT) to obtain the ground-state optimised geometries, and time-dependent DFT (TD-DFT) to evaluate the electronic absorption spectra. Total-energy differences enabled us to evaluate the electron affinities and first and second ionisation energies, the quasiparticle correction to the HOMO–LUMO energy gap and an estimate of the excitonic effects in the neutral molecules. Electronic absorption spectra have been computed by combining two different implementations of TD-DFT: the frequency–space method to study general trends as a function of charge-state and molecular size for the lowest-lying in-plane long-polarised and short-polarised $\pi \rightarrow \pi^*$ electronic transitions, and the real-time propagation scheme to obtain the whole photo-absorption cross-section up to the far-UV. Doubly ionised PAHs are found to display strong electronic transitions of $\pi \rightarrow \pi^*$ character in the near-IR, visible, and near-UV spectral ranges, like their singly charged counterparts. While, as expected, the broad plasmon-like structure with its maximum at about 17–18 eV is relatively insensitive to the charge-state of the molecule, a systematic decrease with increasing positive charge of the absorption cross-section between ∼6 and ∼12 eV is observed for each member of the class.

Keywords: Acenes; Electronic absorption; Density functional theory; Time-dependent density functional theory

1. Introduction

Polycyclic aromatic hydrocarbons [1a,1b] (PAHs) are a large class of conjugated π-electron systems of fundamental importance in many research areas of chemistry as well as in astrophysics and materials science. The carbon skeletons of PAHs may be considered as small pieces of graphite planes and, as such, they have been proposed as precursors to extended carbon networks such as fullerenes and carbon nanotubes [2a,2b]. PAHs are of high interest in environmental chemistry due to their carcinogenicity and their ubiquity as air pollutants produced by the combustion of organic matter [3a,3b]. In the astrophysical context, PAHs are found in carbonaceous meteorites [4a] and in interplanetary dust particles [4b]. Based on the astronomical observation of IR, visible and UV spectroscopic features, neutral and charged PAHs are thought to be the most abundant molecules in space after molecular hydrogen and carbon monoxide [4c].

Oligoacenes, or simply acenes, are a subclass of catacondensed PAHs (with all carbon atoms on the periphery of the ring system) consisting of fused benzene rings joined in a linear arrangement. In their crystalline state these

* Corresponding author. Tel.: +39 070 675 4915; fax: +39 070 510171.
E-mail address: gmalloci@ca.astro.it (G. Malloci).

0301-0104/$ - see front matter © 2007 Elsevier B.V. All rights reserved.
doi:10.1016/j.chemphys.2007.07.046

organic semiconducting materials have received particular attention in the field of electronics and photonics [5a,5b,5c,5d]. Acenes and their derivatives are being increasingly used as active elements in a variety of opto-electronic devices such as organic thin-film field-effect transistors [6a,6b], light-emitting diodes [7a,7b], photovoltaic cells [8a,8b], and liquid crystals [9]. Organic electronics based on functionalised acenes and heteroacenes is presently a very active field of research [10a,10b].

Since the early work by Clar [1a,1b] and Platt [11a,11b], there has been a wide-ranging interest in the electronic properties of PAHs using different spectroscopic techniques, such as absorption [12a,12b,12c,12d,12e,12f,12g, 12h,12i,12j], electron-energy-loss [13a,13b,13c,13d], fluorescence [14a,14b,14c,14d,14e,14f], polarisation [15a,15b, 15c], photoelectron [16a,16b,16c,16d,16e,16f], and photo-ion mass spectrometry [17a,17b,17c,17d]. Thanks to these studies, the electronic spectra of neutral PAHs are known to be composed of two main regions: (i) the broad plasmon-like excitation peaking at ~17–18 eV, which involves $\pi \rightarrow \sigma^*$, $\sigma \rightarrow \pi^*$, $\sigma \rightarrow \sigma^*$, and Rydberg spectral transitions, and (ii) the single-particle excitation part below a few eV, where the lowest energy singlet–singlet $\pi \rightarrow \pi^*$ transitions occur. The four lowest transitions of neutral PAHs are usually described by the Clars's notation p, α, β, β′ [1a], or ^1L_a, ^1L_b, ^1B_b, ^1B_a according to the empirical model of Platt [11a]. In catacondensed PAHs these transitions are characterised by the following intensities and oscillator strengths: p, weak, $f \approx 0.01 - 0.1$; α, very weak, $f \approx 0.001$; β, very strong, $f \approx 1.0$; β′, medium strong, $f \approx 0.1 - 1.0$ (e.g., [17d]). In the case of oligoacenes, in particular, the transition dipole moment for the p-band lies along the short-axis of the molecule, while for the α and β-bands it lies along the long-axis. In the following we will refer to these transitions as "short-polarised" and "long-polarised", respectively.

Charged PAHs have been the subject of extensive spectroscopic studies in frozen glassy organic solids [18a,18b]. These experiments showed that PAH radical cations and anions: (i) display intense optical transitions at lower energies than their parent molecule, and (ii) have very similar electronic spectra, in qualitative agreement with the particle–hole equivalence in the pairing theorem of Hückel's theory [18a]. Currently, the interest on charged PAHs comes mainly from basic research in astrophysics because PAHs are expected to exist in space in different charge states depending on the physical conditions (e.g., UV flux, electron density, etc.) of the host environment [4c]. This has motivated a large amount of laboratory work based first on matrix isolation spectroscopy [19a,19b,19c,19d, 19e,19f,19g,19h,19i,19j,19k] and, more recently, laser mass spectroscopy [20a,20b,20c], spectroscopic studies of the molecules trapped in helium droplets [21a,21b,21c,21d], and a high sensitivity photo-absorption technique in free jets called cavity ring-down spectroscopy [22a,22b,22c, 22d,22e,22f, 22g].

From an astrophysical point of view the knowledge of the electronic absorption spectra of PAHs in all their relevant charge states is of fundamental importance for our understanding of their photophysics in space. While this concerns the whole energetic range excitable in a typical interstellar environment, i.e., from the visible to the far-UV, very few experimental data are available for charged PAHs in this spectral range due to the limitations which are intrinsic to the laboratory techniques more widely used. As a part of a more extensive study [23a,23b,23c,23d,23e] towards the knowledge of the spectral properties of a large sample of PAHs to be modelled in astrophysical environments [24a,24b,24c], we report in this paper a detailed study of the electronic absorption spectra of the five smallest oligoacenes naphthalene, anthracene, tetracene, pentacene, and hexacene in the charge states most relevant for astrophysical applications, i.e., −1, 0, +1, and +2. The geometries of the molecules considered are sketched in Fig. 1. The theoretical methods we used for both ground-state and excited-state calculations have been validated for the basic aromatic unit benzene in its neutral form, for which a large amount of spectroscopic data are available.

There have been many systematic studies of benzenoid hydrocarbons, including acenes, using quantum-chemical calculations to obtain, e.g., heats of formation [25a], infrared spectra [25b], and C–H bond dissociation energies [25c]. While the electronic properties of neutral acenes in the near-IR, visible, and near-UV spectral ranges are thoroughly characterised up to the sizes of hexacene [26a, 26b,26c,26d,26e,26f,26g,26h,26i,26j,26k,27a,27b] and some studies have been done for larger acenes [28a,28b,28c,28d], a comparatively smaller amount of work exists for their corresponding mono-cations [29a,29b,29c,29d,29e,29f, 29g,29h] and mono-anions [29e,29f,30a,30b]. To the best of our knowledge, however, the electronic spectra of charged PAHs in the far-UV spectral domain have not

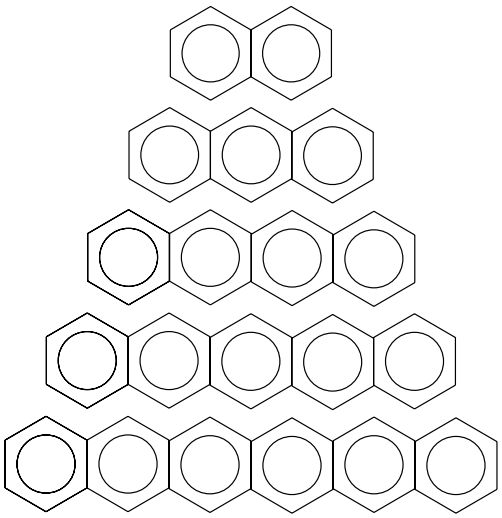

Fig. 1. Oriented geometries of the molecules considered. From top to bottom: naphthalene, anthracene, tetracene, pentacene, and hexacene. The molecules are supposed lying in the x–y plane, the y-axis being the longer one.

been measured to date. In addition, a detailed study of the electronic excitation properties of PAHs in their doubly ionised state has been missing until now. First proposed 20 years ago [31a,31b,31c], the possible presence of PAH dications in the interstellar medium has recently received further support based on the proposition that these molecules could contribute to the luminescence observed in the red part of the visible spectrum in many interstellar sources [32]. While laboratory measurements of the yield of optical fluorescence and phosphorescence by these species are needed to test this hypothesis, the determination of their electronic absorption spectra is motivated.

We used density functional theory (DFT) [33a,33b,33c,33d,33e,33f,33g,33h,33i,33j,33k] and its time-dependent extension (TD-DFT) [34a,34b,34c,34d,34e,34f, 34g,34h,34i,34j,34k], which are methods of choice for this type of investigations for large molecules. Since excitation energies and oscillator strengths within TD-DFT can be computed following two different strategies (see Section 2.2 for details), we used both of them to obtain: (i) the whole absolute photo-absorption cross-sections up to the soft X-ray region near 30 eV, and (ii) the positions, the oscillator strengths, and the leading configurations of the lowest-lying valence $\pi \rightarrow \pi^*$ short-polarised and long-polarised electronic transitions, falling in the visible/near-UV region, as a function of molecular size and charge state. In case (i), due to its numerical stability, we used the adiabatic local-density approximation in the parametrisation of Perdew and Zunger [33c], which has proven to yield reliable results for the dynamical polarisability of conjugated molecules [23e,34g]. In case (ii) we used the hybrid B3LYP functional [33i] and the gradient-corrected BLYP functional [33d,33e], which are widely used in the study of PAHs to obtain a large number of molecular parameters, such as structures and energetics [26a,35a], vibrational spectra [35a,35b,35c], ionisation spectra [26c,26e], ionisation energies [23c,26a,35f,26k], electron affinities [23b,30a,35g,35k], electronic excitations [29d,26d,26f,26g,29f,30b,26k], the vibronic structure of absorption spectra [26h,26i], hydrogen dissociation [29g,29h], and Jahn–Teller effects [35d,35e,35h,35i,35j].

Although the approximate exchange-correlation functionals we used have been developed for the electronic ground-state, they are also routinely employed in TD-DFT calculations, and their application usually yields accurate results for low-lying valence–excited states of both closed-shell [34c,34d] and open-shell [34e,34f] species. It is known, however, that these functionals show the wrong asymptotic behaviour, decaying faster than $1/R$ (i.e., exponentially) for large distances R from the nuclei. Among the well known and documented limitations of these methods [34j,34k] are: (i) the correct description of Rydberg [36a,36b,36c], doubly excited [37a,37b], and charge-transfer [38a,38b,38c] excited-states, (ii) the failure for large, extended π-systems such as polyacetylene fragments and oligoporphyrins [39], and (iii) the system-size-dependent errors found for the lowest short-polarised excited-states (p-bands in Clar's notation) of neutral oligoacenes [26g]. Furthermore, the oscillator strengths computed by TD-DFT are considered to be only in qualitative agreement with experiments. In a rigorous assessment of the quality of TD-DFT molecular oscillator strengths, for example, they were found to be reasonable but not in quantitative agreement with reliable experimental and theoretical values for small molecules such as CO, N_2, and CH_2O [34h].

In spite of the above-mentioned failures of the level of theory we used, it is known to be sufficient to identify the most intense lowest-lying electronic excitations of neutral PAHs [26b,26f] as well as radical ions [29d,29e,29f,30a,30b,40a,40b,40c], which are found to match closely with the available experimental data both in terms of positions and intensity ratios. Despite the non-physical exponential fall-off of the exchange-correlation functional used, in fact, these states all involve excitations to and from delocalised, valence π-orbitals, which are not significantly affected by the shape of the exchange-correlation potentials in the asymptotic region [29f]. In particular, it has been shown that interesting trends exist in the vertical excitation energies and the oscillator strengths for homologous series of PAHs [40a,40b,40c]. For the transitions with the largest oscillator strength in the oligorylenes perylene, terrylene, and quaterrylene, for example, a net increase of the oscillator strength per unit mass of carbon along the series has been found [40a]. This result might have important implications in astrophysics with respect to the long-standing unsolved problem of the diffuse interstellar bands, about 300 unidentified absorption features observed in the near-UV, visible, and near-IR spectra of stars obscured by interstellar dust [41].

Moreover, we used the so-called delta-self-consistent-field (ΔSCF) approach [33g], evaluating total-energy differences between the self-consistent field calculations performed for the neutral and charged systems to obtain: (i) the vertical and adiabatic electron affinities and the first and second ionisation energies; (ii) the quasiparticle correction (quasiparticle energies are associated with the addition or removal of an electron) to the highest occupied molecular orbital (HOMO) – lowest unoccupied molecular orbital (LUMO) gap. This quantity is related to molecular hardness, the analogue of the band gap of solids, defined as half the difference between the ionisation potential and the electron affinity, which is a key property characterising the chemical behaviour and reactivity of a molecule. The comparison between the optical gap, i.e., the lowest singlet–singlet excitation energy obtained with TD-DFT, and the quasiparticle corrected HOMO–LUMO gap enabled us to estimate the excitonic effects (due to the electron–hole interaction) in the neutral molecules.

The paper is organised as follows. Section 2 contains the technical details for the calculation of the ground-state properties (Section 2.1) and the electronic absorption spectra (Section 2.2). The results we obtained are presented in Section 3 and discussed in Section 4. Our concluding remarks are reported in Section 5.

2. Computational details

2.1. DFT calculations

The calculation of the excitation energies and the electronic absorption spectra required the previous knowledge of the ground-state optimised geometries. For this part of the work we used the Gaussian-based DFT module of the NWCHEM package [42]. Geometry optimisations were performed using a basis-set with the smallest addition of diffuse functions, namely the $6-31+G^*$ basis, a valence double zeta set augmented with *d* polarisation functions and *s* and p diffuse functions for each carbon atom.

We used the hybrid B3LYP functional, a combination of the Becke's three parameter exchange functional [33i] and the Lee–Yang–Parr gradient-corrected correlation functional [33e]. Although hybrid DFT functionals are computationally more expensive than other exchange-correlation functionals in the local density or generalised gradient approximations, B3LYP results for ground-state properties are known to be markedly more accurate compared with experiment for a large number of systems including PAHs in general [35a,35b] and oligoacenes in particular [26a,26c,26e,26k]. This is confirmed for neutral benzene, whose optimised bond-lengths we obtain at the B3LYP/$6-31+G^*$ level are $r_{CC}=1.399$ Å, and $r_{CH}=1.087$ Å, to be compared with the empirical equilibrium (r_e) recommended values of, respectively, 1.3914 ± 0.0010 Å and 1.0802 ± 0.0020 Å [43a]. Analogously, the ground-state rotational constant we found is ~5700 MHz, in agreement with the empirical equilibrium (B_e) determination of 5731.73 MHz [43a].

From the structural relaxations performed for both neutral and charged systems, we computed via total-energy differences the adiabatic electron affinities and the adiabatic single and double ionisation energies. At the optimised geometry of the neutral molecule we evaluated also the vertical electron affinity (EA_v) and the vertical first ionisation energy (IE_v). This enabled us to obtain the quasiparticle (QP) corrected HOMO–LUMO gap of the neutral systems considered, which is rigorously defined within the ΔSCF scheme [33g] as

$$QP^1_{gap} = IE_v - EA_v = E_{N+1} + E_{N-1} - 2E_N, \tag{1}$$

E_N being the total energy of the *N*-electron system. We used also the following approximate expression [33f]:

$$QP^2_{gap} = \epsilon^{N+1}_{N+1} - \epsilon^N_N, \tag{2}$$

where ϵ^j_i is the *i*th eigenvalue of the *j*-electron system. The results obtained using the above Eqs. (1) and (2) tend to coincide as the system gets larger and the orbitals more delocalised. The B3LYP/$6-31+G^*$ level of theory shows good agreement with experiments for the electron affinities of PAHs [23b,30a,35k], but it is known to be unable to predict their absolute ionisation energies with chemical accuracy (±0.1 eV) [23c,26a,26k,35f]. This has been discussed in detail by Kadantsev et al. [26k], who concluded that a better description of the electron correlation is needed to reproduce the experimental IEs. Switching to another computational scheme one could employ many-body perturbation theory in the so-called Hedin's GW approximation [44a]. This method, in which the QP energies are calculated from the self-energy operator of the system (given as the product of the Green's function $\mathcal{G}$ and the screened Coulomb interaction *W*), gives results in excellent agreement with the available experiments for many materials (see e.g., [44b]). To assess the reliability of our ΔSCF QP-corrected HOMO–LUMO gaps, we compared them with the GW results obtained for the oligoacenes [28d]. The QP-corrected HOMO–LUMO gap of our benchmark benzene molecule is 10.59 eV ($IE_v=9.20$ eV, $EA_v=-1.39$ eV), that compares favorably with the GW results [28d] of 10.59 eV (first-principles calculations using Gaussian-type orbitals) and 10.46 eV (DFT-based tight-binding calculations), respectively, and with the experimental value of ~10.36 eV ($IE_v=9.24384\pm0.00006$ [43b], $EA_v=-1.12\pm0.03$ eV [43c]).

2.2. TD-DFT calculations

Thanks to the good compromise between accuracy and computational costs, compared to many-electron wavefunction-based *ab initio* methods, TD-DFT is the most widely used approach to compute the excitation energies of such complex molecules as PAHs [26b,26d,26f,26g,26h,26i,28b,29d,29e,29f,30b,40a,40b,40c]. In this study we used two different implementations of TD-DFT in the linear response regime, in conjunction with different representations of the wavefunctions:

(1) the real-time propagation scheme using a grid in real space [34g], as implemented in the OCTOPUS computer program [45a,45b,45c,45d].
(2) the frequency–space implementation [34e] based on the linear combination of localised orbitals, as given in the NWCHEM package [42].

In the first scheme (1) the time-dependent Kohn–Sham equations are directly solved in real-time and the wavefunctions are represented by their discretised values on a uniform spatial grid. The static Kohn–Sham wavefunctions are perturbed by an impulsive electric field and propagated for a given finite time interval. In this way, all of the frequencies of the system are excited. The whole absolute photo-absorption cross-section $\sigma(E)$ then follows from the dynamical polarisability $\alpha(E)$, which is related to the Fourier transform of the time-dependent dipole moment of the molecule. The relation is

$$\sigma(E) = \frac{8\pi^2 E}{hc}\,\Im\{\alpha(E)\}, \tag{3}$$

where *h* is Planck's constant, $\Im\{\alpha(E)\}$ is the imaginary part of the dynamical polarisability, and *c* the velocity of light in

vacuum. The dipole strength-function $S(E)$ is related to $\sigma(E)$ by the equation:

$$S(E) = \frac{m_e c}{\pi h e^2}\sigma(E), \quad (4)$$

m_e and e being respectively the mass and charge of the electron. $S(E)$ has units of oscillator strength per unit energy and satisfies the Thomas–Reiche–Kuhn dipole sum-rule $N_e = \int dE S(E)$, where N_e is the total number of electrons. The great advantage of obtaining the whole response at once is particularly useful for astrophysical applications, for which the whole absorption spectrum is needed.

In the most widely used frequency–space TD-DFT implementation (2), based on the linear response of the density–matrix, the poles of the linear response function correspond to vertical excitation energies and the pole strengths to the corresponding oscillator strengths [34b]. With this method computational costs scale steeply with the number of required transitions and electronic excitations are thus usually limited to the low-energy part of the spectrum. From a computational point of view the advantages of the real-time propagation method are discussed, e.g., in Ref. [45d]. On the other hand, the main drawbacks of the real-time approach are that: (i) no information is given on dipole-forbidden singlet–singlet and singlet–triplet transitions, and (ii) one does not obtain independent information for each excited state, such as its irreducible representation of the point group of the given molecular system, and the description of the excitations in terms of promotion of electrons in an orbital picture.

We performed the OCTOPUS calculations in the local-density approximation, with the exchange-correlation energy density of the homogeneous electron gas [46a] parametrised by Perdew and Zunger [33c]. The ionic potentials are replaced by norm-conserving pseudo-potentials [46b]. We used a grid spacing of 0.3 Å and determined the box size by requiring each atom to be at least 4 Å away from its edges. We furthermore added a 1 Å thick absorbing boundary, which quenches spurious resonances due to standing waves in the finite simulation box used to confine the molecules [34g,45c]. We used a time integration length $T = 20\hbar$ eV, corresponding to an energy resolution of $\hbar/T = 0.05$ eV. For the numerical integration of the time evolution we used a time step of $0.002\hbar$ eV, which ensured energy conservation with good numerical accuracy.

The TD-DFT calculations with NWCHEM were performed at the same level B3LYP/$6-31+G^*$ used to obtain the ground-state geometries. Although basis set convergence is not yet expected at the level we used, our results for the neutral systems are almost coincident with the ones obtained in Ref. [26k] using the larger $6-311{+}{+}G^{**}$ basis, which is supplemented with a third layer of valence functions and includes polarisation and diffuse functions on both carbon and hydrogen atoms. We thus believe our theoretical predictions to be sufficiently accurate for the purposes of this work. In the case of neutral benzene, we predict the strong $\pi \rightarrow \pi^*$ transition $^1A_{1g} \rightarrow {}^1E_{1u}$ at 6.96 eV with an oscillator strength of 1.22, in good agreement with the measured band position in vapour-phase of 6.94 eV with an f-value of 1.2 [43d].

In order to assess the choice of this specific exchange-correlation functional, at the B3LYP optimised geometries, we used also the gradient-corrected BLYP functional [33d,33e], the same approach used in previous studies of PAH ions [29d,40a,29f,30b]. With both methods we restricted ourselves to the first 20 singlet–singlet roots. Since we are interested in the behaviour of the lowest-lying permitted in-plane long-polarised and short-polarised electronic transitions as a function of charge-state and molecular size, in the following we report only the first five electronic transitions. The complete set of electronic excitation energies and oscillator strengths computed at both B3LYP and BLYP levels, including also the optically inactive ones, are available in our online database of the computed spectral properties of PAHs [23d].

3. Results

3.1. Static properties

Geometry optimisations with NWCHEM were performed using tight convergence criteria, that are specified by maximum and root mean square gradient thresholds of 1.5×10^{-5} and 1.0×10^{-5} atomic units, respectively, and maximum and root mean square thresholds of the Cartesian step respectively of 6.0×10^{-5} and 4.0×10^{-5} atomic units. According to previous studies [29b,29d] the lifting of the molecular symmetry D_{2h} of the neutral molecules is not expected to lead to optimised geometries with lower symmetry for the corresponding charged species. We indeed confirmed that the structural parameters obtained for naphthalene, anthracene, and tetracene in the charge-states -1,$+1$, and $+2$, ignoring any apparent symmetry and adopting the D_{2h} symmetry, are coincident within numerical errors. We therefore assumed the above D_{2h} constraint for all subsequent calculations in the paper. Our B3LYP/$6-31+G^*$ geometry optimisations for the neutral molecules give structural parameters in good agreement with those previously published [26a,26e,26k]. In particular, although a larger basis was used in Ref. [26k], the two sets of results are almost coincident and compare fairly well with the available X-ray data. We do not discuss here the changes of the single bond lengths and bond angles occurring in the charged species, compared to the corresponding neutral ones. Depictions of the structures of each molecule considered, in which internal coordinates are shown and compared, are given as supplementary material to the paper. Instead, Fig. 2 presents in a collective way the structural variations relative to the neutral molecules, expressed in terms of the percentage variations of the rotational constants A and B. These latter quantities are proportional to the inverse of the principal momenta of inertia corresponding to the in-plane short and long-axis

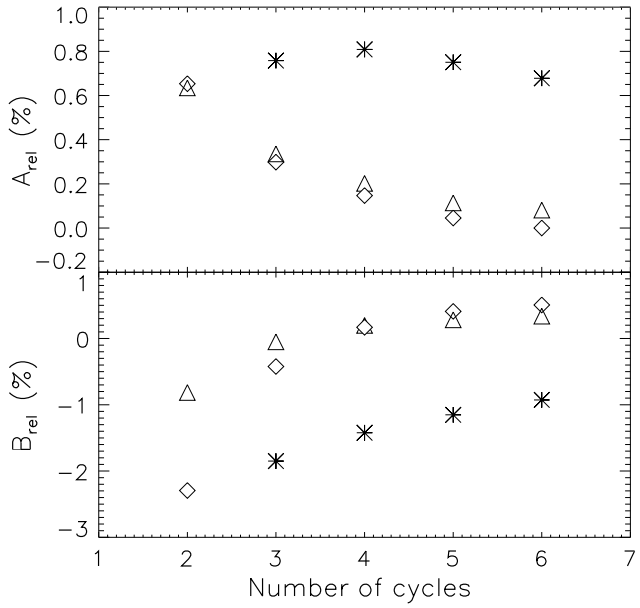

Fig. 2. Percentage variation of the rotational constants A (top panel) and B (bottom panel) relative to the neutral counterparts for anions (asterisks), cations (triangles), and dications (diamonds), as a function of molecular size. We omit the entries for naphthalene anion, which is known not to form a stable anion in the gas-phase.

of the molecules, respectively: $A = (h/8\pi^2 c)I_{\text{short}}$, $B = (h/8\pi^2 c)I_{\text{long}}$. Note that in Fig. 2 we omitted the results corresponding to naphthalene anion, since gas-phase naphthalene is unable to bind an additional electron in its LUMO state [43c]. The ground-state optimised geometries of all of the molecules considered, both Cartesian and internal coordinates, are freely available in our online database of the computed spectral properties of PAHs [23d].

All neutral and singly charged species were computed as singlet and doublet, respectively, while for dications we computed both their singlet and triplet ground-states. The adiabatic and vertical values of electron affinities and single and double ionisation energies as obtained via total-energy differences are given in Table 1 and compared with the available experimental data [47,31c]. As shown in Table 1, for all of the five molecules considered in their doubly ionised state, our calculations predict the total energy of the singlet state to be lower than that of the triplet state by ~0.5–1.0 eV. Fig. 3 displays the computed electron affinities and first and double ionisation energies as a function of size, and compares them with the available laboratory data.

3.2. Excitation energies and electronic absorption spectra

Since its first applications, the real-time TD-DFT method in real space was proven to give good results for neutral benzene [34g,45c], compared with the experimental spectrum recorded in the energy range 6–35 eV [12e]. Applying this same approach to a large sample of PAHs, we already showed [23a,24b] our results to be in good agreement up to photon energies of about 30 eV with the experimental data obtained for a few neutral PAHs with the synchrotron radiation facility of SUPERACO [12h,12i]. The comparison between the theoretical spectra obtained with the OCTOPUS code and the experimental photo-absorption cross-sections of neutral anthracene ($C_{14}H_{10}$) and benzene in the gas-phase are shown in Figs. 4 and 5. The latter experimental spectra are in good agreement with the ones obtained with the synchrotron radia-

Table 1
Adiabatic and vertical values (in parentheses), all data in eV, of electron affinities and single and double ionisation energies of the oligoacenes considered in this work ($C_{4n+2}H_{2n+4}$, $n = 2, 3, 4, 5, 6$) as obtained through total-energy differences at the B3LYP/6 − 31 + G* level

Number of cycles	Electron affinity		First ionisation energy		Dication state	Double ionisation energy	
	Ad. (Vert.)	Exp.	Ad. (Vert.)	Exp.		Ad. (Vert.)	Exp.
2	−0.26(−0.38)	−0.20 ± 0.05[a]	7.80(7.89)	8.144 ± 0.001[b]	Singlet Triplet	20.99(21.35) 21.45(21.57)	21.5 ± 0.2
3	0.53(0.43)	0.530 ± 0.005[c]	7.02(7.09)	7.439 ± 0.006[d]	Singlet Triplet	18.70(18.95) 19.70(19.80)	–
4	1.08(1.00)	1.067 ± 0.043[e]	6.49(6.55)	6.97 ± 0.05[f]	Singlet Triplet	17.15(17.34) 17.96(18.11)	18.6 ± 0.2
5	1.48(1.41)	1.392 ± 0.043[e]	6.12(6.16)	6.589 ± 0.001[g]	Singlet Triplet	16.03(16.18) 16.67(16.80)	17.4 ± 0.2
6	1.78(1.72)	–	5.83(5.87)	6.36 ± 0.02[f]	Singlet Triplet	15.18(15.30) 15.68(15.78)	–

For comparison we list also the experimental adiabatic electron affinities and adiabatic single ionisation energies taken from the NIST Chemistry WebBook [47], as well as the adiabatic second ionisation energies photon-impact measurements [31c].

[a] Extrapolated from the EAs of naphthalene–water clusters determined via photoelectron spectroscopy [16e].
[b] From laser threshold photoelectron spectroscopy [16c].
[c] From photodetachment photoelectron spectroscopy [16d].
[d] From two-laser photoionisation supersonic jet mass spectrometry [17a].
[e] Estimated from gas-phase electron attachment free energies with the electron-transfer equilibria technique [48].
[f] From gas-phase photoelectron spectroscopy [16b].
[g] From high-resolution gas-phase photoelectron spectroscopy [16f].

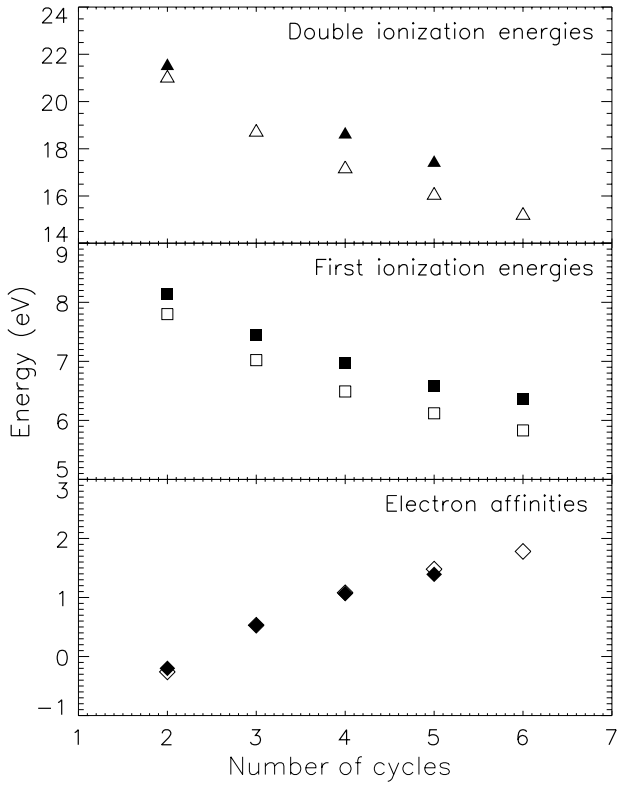

Fig. 3. Computed adiabatic ionisation energies and electron affinities of the studied oligoacenes as a function of size. The corresponding experimental values are represented by the filled symbols (see Table 1).

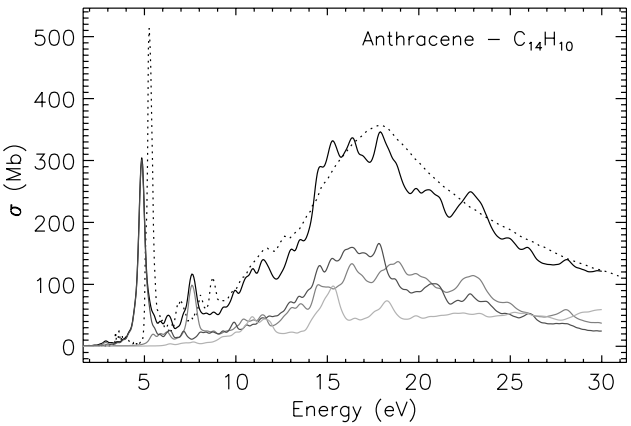

Fig. 4. Comparison between the computed (solid black line) photo-absorption cross-section $\sigma(E)$ of neutral anthracene ($C_{14}H_{10}$) and the corresponding gas-phase absorption spectrum (dotted line, taken from Refs. [12h,12i]). The contributions corresponding to polarisations along the x-axis (in-plane short), y-axis (in-plane long), and z-axis (out-of-plane), are marked in gray, dark gray, and light gray, respectively. Units are megabarns, 1 Mb = 10^{-18} cm^2.

tion from the electron accelerator DESY for anthracene [12g], and benzene [12e], respectively. Since the theoretical spectrum is averaged over the three x, y, and z polarisations, each single contribution is also shown in Figs. 4 and 5. As examples, the spectra computed for tetracene ($C_{18}H_{12}$) and pentacene ($C_{22}H_{14}$) in the four charge states considered are given in Figs. 6 and 7. The spectra for all

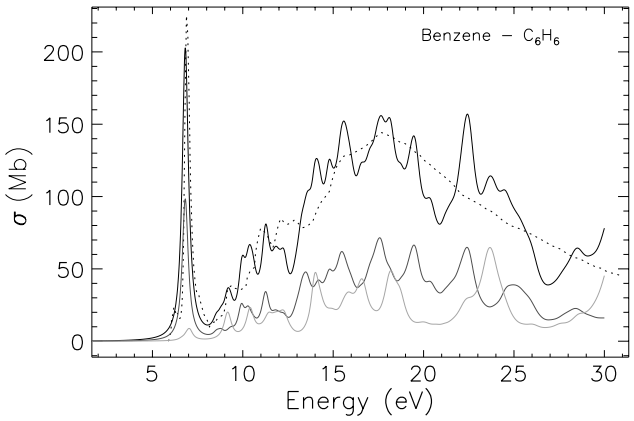

Fig. 5. Same as Fig. 4 for neutral benzene. Note that, due to the symmetry of the molecule, the curves corresponding to x and y polarisations are obviously coincident.

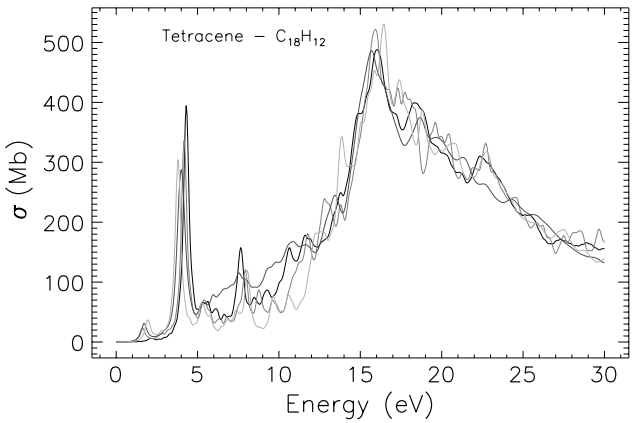

Fig. 6. Computed photo-absorption cross-section $\sigma(E)$ of tetracene ($C_{18}H_{12}$) in neutral (black), anionic (dark gray), cationic (gray) and dicationic (light gray) charge-state, as obtained with the real-time real-space implementation of TD-DFT.

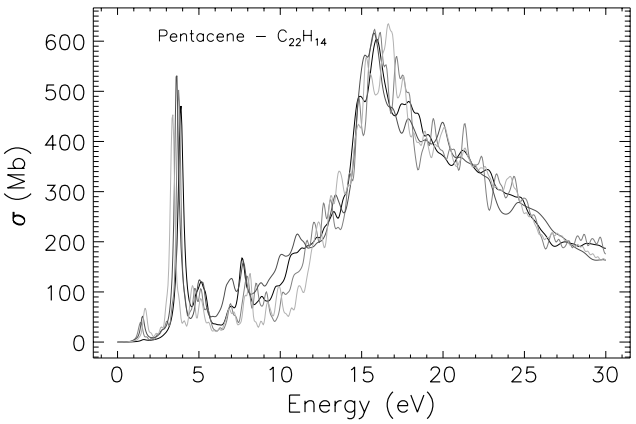

Fig. 7. Same as Fig. 6 for pentacene ($C_{22}H_{14}$).

of the other molecules under study can be found in our online database [23d]. Fig. 8 shows the comparison between the integrated values in the range 6–12 eV of the

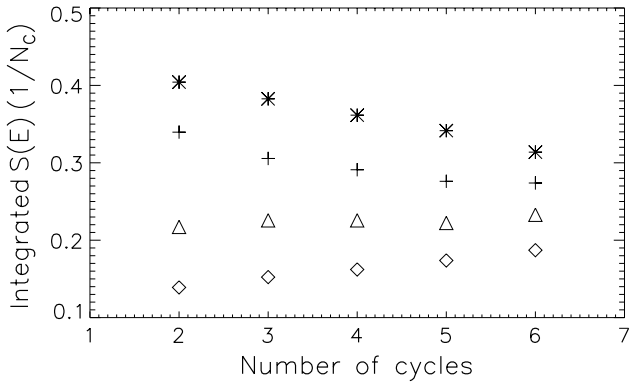

Fig. 8. Comparison between the integrated values in the range 6–12 eV of the individual dipole strength-functions $S(E)$ (see Eq. (4)) divided by the number of carbon atoms for the oligoacenes anions (asterisks), neutrals (crosses), cations (triangles), and dications (diamonds) considered, as a function of molecular size.

individual dipole strength-functions $S(E)$ (see Eq. (4)) divided by the number of carbon atoms in each molecule as a function of molecular size.

The first few permitted electronic transitions of each molecule, as obtained at the B3LYP/$6-31+G^*$ and BLYP//B3LYP/$6-31+G^*$ levels with the TD-DFT frequency–space implementation of NWCHEM are reported in Tables 2–6, and compared with the available experimental data that we could find in the literature. We deliberately omitted the large amount of photoelectron data available for neutral species [16a,16b,16c,16d,16e,16f]. The use of such data for spectral assignments of the so-called Koopmans transitions of radical cations has been already discussed many times [29c,29d,29e,29f]. Electronic excited states are classified under the point-group D_{2h} and the ground-state symmetry is specified for each charge-state. As to the character of the excited electronic states, we analyse the nature of the corresponding transitions in terms of the occupied and virtual molecular orbitals that have been interchanged between the ground and the excited electronic states [34j]. The above description is computationally convenient and straightforward for states which are well described with only one or two significantly contributing "excited" Slater determinants [34j]. This is the case for the electronic excited states reported in Tables 2–6. The

Table 2
Singlet–singlet lowest-lying permitted excitation energies (in eV) of naphthalene anion, neutral, cation, and dication as obtained via frequency–space TD-DFT

State (pol.)	Excitation	BLYP	B3LYP	Exp.
Anion (ground-state $^2B_{3g}$)				
$1\ ^2B_{2u}$ (z)	$\pi_0 \rightarrow \pi_2^*$	0.66(0.001)	0.99(0.001)	–
$1\ ^2B_{1u}$ (y)	$\pi_0 \rightarrow \pi_7^*$	1.48(0.022)	1.58(0.034)	~1.5[a]
$2\ ^2B_{2u}$ (z)	$\pi_0 \rightarrow \pi_8^*$	1.85(0.005)	2.15(0.006)	–
$2\ ^2B_{1u}$ (y)	$\pi_0 \rightarrow \sigma_2^*$	2.30(0.071)	2.49(0.069)	~2.5[a]
$1\ ^2A_u$ (x)	$\pi_{-1} \rightarrow \pi_1^*$	2.73(0.001)	2.89(<0.001)	–
Neutral (ground-state ^1A_g)				
$1\ ^1B_{3u}$ (x, p)	$\pi_{-1} \rightarrow \pi_1^*$	4.06(0.045)	4.36(0.061)	4.45(0.102)[b], 4.45(0.109)[c], 4.44[d]
$1\ ^1B_{2u}$ (y, α)	$\pi_{-2} \rightarrow \pi_1^*$, $\pi_{-1} \rightarrow \pi_2^*$	4.20(<0.001)	4.44(<0.001)	3.97(0.002)[b], 4.0[c], 3.98[d]
$2\ ^1B_{2u}$ (y, β)	$\pi_{-2} \rightarrow \pi_1^*$, $\pi_{-1} \rightarrow \pi_2^*$	5.62(1.155)	5.85(1.260)	5.89(1.3)[b], 5.89(1.3)[c], 5.86[d]
$2\ ^1B_{3u}$ (x)	$\pi_{-2} \rightarrow \pi_2^*$	5.80(0.146)	6.08(0.199)	6.14(0.3)[b], 6.0[c], 6.09[d]
$1\ ^1B_{1u}$ (z)	$\pi_{-2} \rightarrow \pi_3^*$	5.77(0.008)	6.24(0.016)	–
Cation (ground-state ^2A_u)				
$1\ ^2B_{2g}$ (y)	$\pi_{-2} \rightarrow \pi_0^*$	2.15(0.042)	2.14(0.053)	1.84[d], 1.85(0.052)[e], 1.84(0.011)[f]
$1\ ^2B_{3g}$ (x)	$\pi_{-3} \rightarrow \pi_0^*$	2.77(0.006)	2.98(0.006)	2.72[d], 2.72(0.010)[e], 2.69(0.001)[f]
$2\ ^2B_{3g}$ (x)	$\pi_0 \rightarrow \pi_1^*$	3.51(0.051)	3.59(0.064)	3.29[d], 3.25(0.016)[f]
$2\ ^2B_{2g}$ (y)	$\pi_{-1} \rightarrow \pi_1^*$	3.74(0.012)	3.91(0.032)	4.02[d], 4.03(0.024)[f]
$3\ ^2B_{2g}$ (y)	$\pi_0 \rightarrow \pi_2^*$	4.30(0.008)	4.61(0.006)	4.49[d], 4.52(0.060)[f]
Dication (ground-state ^1A_g)				
$1\ ^1B_{2u}$ (y)	$\pi_{-2} \rightarrow \pi_1^*$	2.85(0.061)	3.00(0.090)	–
$1\ ^1B_{1u}$ (z)	$\pi_{-4} \rightarrow \pi_1^*$	2.71(<0.001)	3.25(<0.001)	–
$1\ ^1B_{3u}$ (x)	$\pi_{-3} \rightarrow \pi_1^*$	3.32(0.062)	3.67(0.090)	–
$2\ ^1B_{2u}$ (y)	$\pi_{-1} \rightarrow \pi_2^*$	5.06(0.833)	5.28(0.865)	–
$2\ ^1B_{1u}$ (z)	$\sigma_{-3} \rightarrow \pi_1^*$	4.95(0.001)	5.58(0.002)	–

The corresponding oscillator strengths are given in parentheses. Polarisation of the bands are denoted according to Fig. 1 as x, y, and z for in-plane short, in-plane long, and out-of-plane polarised bands, respectively. The description of each excitation is based on the B3LYP results and is given in terms of the occupied and virtual molecular orbitals contributing significantly to it [29d,29f]. We report also the available experimental data for comparison.

[a] Absorption in glassy organic solid [18a].
[b] Gas-phase absorption [12c].
[c] Electron-energy-loss spectroscopy [13b].
[d] Absorption in neon-matrix [19d].
[e] Gas-phase absorption [20b].
[f] Absorption in argon-matrix [19b].

Table 3
Same as Table 2 for anthracene in its −1, 0, +1, and +2 charge-states

State (pol.)	Excitation	BLYP	B3LYP	Exp.
Anion (ground-state $^2B_{1u}$)				
$1\ ^2A_g$ (z)	$\pi_0 \rightarrow \pi_1^*$	1.23(0.001)	1.56(0.001)	–
$1\ ^2B_{3g}$ (y)	$\pi_0 \rightarrow \pi_5^*$	1.83(0.110)	1.90(0.137)	∼1.7[a]
$2\ ^2A_g$ (z)	$\pi_0 \rightarrow \pi_7^*$	1.88(0.001)	2.17(0.002)	–
$1\ ^2B_{2g}$ (x)	$\pi - 1 \rightarrow \pi_0^*$	2.12(0.008)	2.20(0.012)	∼2.4[a]
$2\ ^2B_{2g}$ (x)	$\pi_0 \rightarrow \pi_{11}^*$	2.78(0.008)	3.01(0.010)	–
Neutral (ground-state ^1A_g)				
$1\ ^1B_{3u}$ (x, p)	$\pi_{-1} \rightarrow \pi_1^*$	2.92(0.039)	3.21(0.058)	3.27(0.1)[b], 3.45[c], 3.43[d]
$1\ ^1B_{2u}$ (y, α)	$\pi_{-2} \rightarrow \pi_1^*$, $\pi_{-1} \rightarrow \pi_2^*$	3.60(<0.001)	3.85(<0.001)	3.47–3.60–3.45[e], 3.84[f]
$2\ ^1B_{3u}$ (x)	$\pi_{-1} \rightarrow \pi_6^*$	4.59(<0.001)	5.06(<0.001)	–
$2\ ^1B_{2u}$ (y, β)	$\pi_{-2} \rightarrow \pi_1^*$, $\pi_{-1} \rightarrow \pi_2^*$	4.88(1.782)	5.14(1.992)	4.84(2.28)[b], 5.24[c]
$1\ ^1B_{1u}$ (z)	$\pi_{-1} \rightarrow \pi_7^*$	4.83(0.001)	5.24(0.002)	–
Cation (ground-state $^2B_{2g}$)				
$1\ ^2A_u$ (y)	$\pi_{-2} \rightarrow \pi_0^*$	1.87(0.085)	1.93(0.108)	1.71[a], 1.73(0.076)[g], 1.75[h]
$1\ ^2B_{1u}$ (x)	$\pi_0 \rightarrow \pi_1^*$	2.21(0.004)	2.32(0.007)	2.02(0.018)[g]
$2\ ^2B_{1u}$ (x)	$\pi_{-4} \rightarrow \pi_0^*$	2.91(0.044)	3.17(0.058)	2.83[a], 2.90(0.026)[g]
$2\ ^2A_u$ (y)	$\pi_{-1} \rightarrow \pi_1^*$	3.22(0.017)	3.39(0.054)	3.52(0.104)[g]
$3\ ^2A_u$ (y)	$\pi_0 \rightarrow \pi_2^*$	3.69(0.016)	4.02(0.010)	3.95(0.187)[g]
Dication (ground-state ^1A_g)				
$1\ ^1B_{2u}$ (y)	$\pi_{-2} \rightarrow \pi_1^*$	2.31(0.139)	2.45(0.206)	–
$1\ ^1B_{3u}$ (x)	$\pi_{-3} \rightarrow \pi_1^*$	3.02(0.052)	3.39(0.078)	–
$2\ ^1B_{2u}$ (y)	$\pi_{-1} \rightarrow \pi_2^*$	4.38(1.368)	4.63(1.444)	–
$1\ ^1B_{1u}$ (z)	$\pi_{-8} \rightarrow \pi_1^*$	3.92(<0.001)	4.66(<0.001)	–
$2\ ^1B_{3u}$ (x)	$\pi_{-4} \rightarrow \pi_2^*$	4.96(0.002)	5.59(0.001)	–

[a] Absorption in glassy organic solid [18a].
[b] Absorption in *n*-heptane solution [11b].
[c] Gas-phase absorption [12g].
[d] Fluorescence jet spectroscopy [14b].
[e] Magnetic circular dichroism measurements in solvents [15a,15b,15c].
[f] Two-photon absorption in solution [12d].
[g] Absorption in argon-matrix [19e].
[h] Gas-phase absorption [22d].

use of more sophisticated and physically more appealing ways to obtain information about an electronic transition, such as difference density or attachment/detachment density plots [34j], is outside the scope of the present work. We used the same notation as in Refs. [29d,29f] where the π orbitals are numbered in the order of increasing energies and π_{-1}, $\pi_0(\pi_0^*)$, and π_1^* denote the highest doubly occupied π orbital, the singly occupied (unoccupied) π orbital, and the lowest doubly unoccupied π orbital, respectively.

Figs. 9 and 10 display, respectively, the B3LYP/$6-31+G^*$ positions and the corresponding oscillator strengths of the lowest in-plane short-polarised (p-bands in the neutral molecules) and long-polarised (α-bands in the neutral molecules) electronic transitions as a function of the number of benzene units and the charge-state of the molecule.

3.3. Quasiparticle-corrected HOMO–LUMO gap of the neutral species

For each of the neutral molecules considered at the B3LYP/$6-31+G^*$ level, we report in Table 7 the comparison between the HOMO–LUMO gap E_{gap}^{KS} obtained as difference of Kohn–Sham eigenvalues, the excitation energy of the HOMO–LUMO transition $E_{gap}^{TD\text{-}DFT}$ as given by TD-DFT, and the corresponding experimental value E_{gap}^{exp} (p-bands in Tables 2–6). In the same table we compare the results of Eqs. (1) and (2) with the DFT-based tight-binding GW data of Ref. [28d], $QP_{gap}^{DFT\text{-}GW}$, as well as with the corresponding experimental value obtained as the difference between the experimental EAs and first IEs given in Table 1, $QP_{gap}^{exp} = IE_{exp} - EA_{exp}$. The theoretical exciton binding energy E_{bind} is estimated through the difference $QP_{gap}^{1} - E_{gap}^{TD\text{-}DFT}$, which is compared with its corresponding experimental value $QP_{gap}^{exp} - E_{gap}^{exp}$. All of these quantities are displayed in Fig. 11 as a function of molecular size.

4. Discussion

Fig. 2 shows that structural variations between charged species and their respective neutral counterparts display the same well-defined trend as a function of molecular size: a general decrease for A_{rel} (with the possible exception of anthracene anion), and an increase of B_{rel} is observed for all charge-states considered. More specifically, the largest structural changes are observed for the anions, a consequence of the strongly antibonding character of the LUMO

Table 4
Same as Table 2 for tetracene in its −1, 0, +1, and +2 charge-states

State (pol.)	Excitation	BLYP	B3LYP	Exp.
Anion (ground-state $^2B_{3g}$)				
$1\ ^2A_u$ (x)	$\pi_{-1} \rightarrow \pi_0^*$	1.53(0.009)	1.60(0.014)	1.69[a]
$1\ ^2B_{1u}$ (y)	$\pi_0 \rightarrow \pi_1^*$	1.68(0.164)	1.77(0.209)	1.50[a]
$1\ ^2B_{2u}$ (z)	$\pi_0 \rightarrow \pi_3^*$	1.68(0.001)	2.06(0.001)	1.91[a]
$2\ ^2B_{1u}$ (y)	$\pi_0 \rightarrow \pi_{10}^*$	2.40(<0.01)	2.62(<0.001)	–
$2\ ^2B_{2u}$ (z)	$\pi_0 \rightarrow \pi_{11}^*$	2.58(0.001)	2.91(0.001)	–
Neutral (ground-state ^1A_g)				
$1\ ^1B_{3u}$ (x, p)	$\pi_{-1} \rightarrow \pi_1^*$	2.16(0.031)	2.45(0.049)	2.62(0.08)[b], 2.60(0.11)[c], 2.72[d]
$1\ ^1B_{2u}$ (y, α)	$\pi_{-3} \rightarrow \pi_1^*$, $\pi_{-1} \rightarrow \pi_3^*$	3.21(0.001)	3.47(0.002)	3.12[d]
$2\ ^1B_{3u}$ (x)	$\pi_{-1} \rightarrow \pi_5^*$	3.98(<0.001)	4.59(<0.001)	–
$2\ ^1B_{2u}$ (y, β)	$\pi_{-3} \rightarrow \pi_1^*$, $\pi_{-1} \rightarrow \pi_3^*$	4.34(2.317)	4.62(2.691)	4.55(1.85)[b], 4.50(1.75)[c]
$3\ ^1B_{3u}$ (x)	$\pi_{-4} \rightarrow \pi_1^*$	4.35(0.010)	4.92(<0.001)	–
Cation (ground-state ^2A_u)				
$1\ ^2B_{2g}$ (y)	$\pi_{-1} \rightarrow \pi_0^*$	1.59(0.129)	1.70(0.169)	1.43[a], 1.43[e]
$1\ ^2B_{3g}$ (x)	$\pi_0 \rightarrow \pi_1^*$	1.58(0.008)	1.70(0.012)	1.65[a], 1.66[e]
$2\ ^2B_{3g}$ (x)	$\pi - 4 \rightarrow \pi_0^*$	2.67(0.029)	3.03(0.041)	3.14[a], 3.16[e]
$2\ ^2B_{2g}$ (y)	$\pi - 2 \rightarrow \pi_1^*$	2.81(0.025)	3.05(0.084)	–
$3\ ^2B_{2g}$ (y)	$\pi - 5 \rightarrow \pi_0^*$	3.17(0.005)	3.52(0.005)	–
Dication (ground-state ^1A_g)				
$1\ ^1B_{2u}$ (y)	$\pi_{-1} \rightarrow \pi_1^*$	1.97(0.226)	2.11(0.335)	–
$1\ ^1B_{3u}$ (x)	$\pi_{-4} \rightarrow \pi_1^*$	2.80(0.042)	3.16(0.065)	–
$2\ ^1B_{2u}$ (y)	$\pi_{-5} \rightarrow \pi_1^*$	3.65(0.093)	4.05(0.626)	–
$1\ ^1B_{1u}$ (z)	$\pi_{-8} \rightarrow \pi_1^*$	3.46(<0.001)	4.11(<0.001)	–
$3\ ^1B_{2u}$ (y)	$\pi_{-2} \rightarrow \pi_2^*$	3.86(1.709)	4.16(1.353)	–

[a] Absorption in glassy organic solid [18a].
[b] Absorption in *n*-heptane solution [11b].
[c] Absorption in benzene solution [12a].
[d] Absorption in gas-phase [14a].
[e] Absorption in argon-matrix [19c,19g].

of the neutral counterpart. The variations in both cations and dications are nearly equal and remain small. A shortening along the short-axis ($A_{rel} > 0$) compared to the neutral molecules is always observed. The anions appear to be primarily distorted along the long-axis showing a lengthening along it ($B_{rel} < 0$) for all sizes. These findings agree with a Hartree–Fock study of naphthalene and anthracene cations [25b], and a DFT study of anthracene anion performed with both hybrid and gradient-corrected exchange-correlation functionals [30a].

Table 1 and Fig. 3 confirm for the oligoacenes the good agreement found for the whole class of PAHs between the B3LYP/$6-31+G^*$ electron affinities and the available experimental data. The differences between computed and observed first ionisation energies are of the same order of magnitude as in previous analyses [26a,26k], and seem to increase slightly at increasing molecular size (from ∼4% for naphthalene to ∼10% for hexacene). Double ionisation energies are found to change more rapidly along the series than single ionisation energies, and the relative errors of our calculations, in comparison with the only three experimental data available, increase from ∼2% for naphthalene to ∼8% for anthracene and tetracene.

As shown in Figs. 4 and 5, the real-time real-space TD–DFT method provides results in very good agreement with the available experimental data for neutral species up to about 30 eV. The broad plasmon-like excitation peaking at about 17.5 eV, which involves $\pi \rightarrow \sigma^*$, $\sigma \rightarrow \pi^*$, $\sigma \rightarrow \sigma^*$, and Rydberg spectral transitions, is well reproduced both in position and width. However, as previously discussed in the case of neutral benzene [34g], the use of the finite simulation box and the absorbing boundary at its edges does not give a satisfactory treatment of continuum effects producing spurious structures. The contribution of the three possible polarisations to the total absorption cross-section varies considerably. While the low-energy part is due to in-plane-polarised electronic transitions (x and y axes), the contribution of the z-axis perpendicular to the plane of the molecule is significant only above a few eV. These features are found to be common to all PAHs [23a,23b,23c,23d,23e]. In the case of oligoacenes, due to their special symmetry, the strongest absorption (β band in the neutral molecules) corresponds to long-axis polarisation, which can be simply understood as the classical resonance in a conducting rod [11a]. From Figs. 6 and 7 it is seen that the broad plasmon-like structure with its maximum at 17–18 eV is relatively insensitive to the charge-state of the molecule. On the other hand, the charge-state of the molecule shows up in the low-energy range and, interestingly, the onset of this broad absorption moves blue-ward and becomes steeper with increasing positive charge. As shown in Fig. 8 this translates into a sys-

Table 5
Same as Table 2 for pentacene in its −1, 0, +1, and +2 charge-states

State (pol.)	Excitation	BLYP	B3LYP	Exp.
Anion (ground-state $^2B_{1u}$)				
1 $^2B_{2g}$ (x)	$\pi_{-1} \rightarrow \pi_0^*$	1.10(0.008)	1.16(0.013)	1.06[a], 1.37[c]
1 $^2B_{3g}$ (y)	$\pi_0 \rightarrow \pi_1^*$	1.50(0.224)	1.60(0.286)	1.40[a], 1.42[c]
1 ^2A_g (z)	$\pi_0 \rightarrow \pi_3^*$	1.96(0.001)	2.35(0.001)	–
2 ^2A_g (z)	$\pi_0 \rightarrow \pi_8^*$	2.53(<0.001)	2.81(0.001)	–
2 $^2B_{3g}$ (y)	$\pi - 1 \rightarrow \pi_4^*$	2.65(0.016)	2.86(0.118)	2.82[a]
Neutral (ground-state ^1A_g)				
1 $^1B_{3u}$ (x,p)	$\pi_{-1} \rightarrow \pi_1^*$	1.63(0.023)	1.91(0.041)	2.12(0.08)[b], 2.28[c], 2.31[d]
1 $^1B_{2u}$ (y,α)	$\pi_{-3} \rightarrow \pi_1^*$, $\pi_{-1} \rightarrow \pi_3^*$	2.94(0.004)	3.21(0.005)	3.73[c]
2 $^1B_{3u}$ (x)	$\pi_{-4} \rightarrow \pi_1^*$	3.33(<0.001)	3.95(<0.001)	–
2 $^1B_{2u}$ (y,β)	$\pi_{-3} \rightarrow \pi_1^*$, $\pi_{-1} \rightarrow \pi_3^*$	3.93(2.706)	4.24(3.346)	4.00(2.20)[b], 4.40[c]
3 $^1B_{3u}$ (x)	$\pi_{-1} \rightarrow \pi_4^*$	3.66(0.021)	4.26(0.003)	–
Cation (ground-state $^2B_{2g}$)				
1 $^2B_{1u}$ (x)	$\pi_0 \rightarrow \pi_1^*$	1.17(0.007)	1.25(0.012)	1.27[c]
1 ^2A_u (y)	$\pi_{-1} \rightarrow \pi_0^*$	1.42(0.182)	1.50(0.238)	1.31[c]
2 ^2A_u (y)	$\pi_{-2} \rightarrow \pi_1^*$	2.61(0.034)	2.80(0.122)	2.92[c]
2 $^2B_{1u}$ (x)	$\pi_{-4} \rightarrow \pi_0^*$	2.60(0.019)	2.85(0.013)	–
2 $^2B_{1u}$ (x)	$\pi_{-4} \rightarrow \pi_0^*$	2.85(0.001)	3.10(0.022)	–
Dication (ground-state ^1A_g)				
1 $^1B_{2u}$ (y)	$\pi_{-1} \rightarrow \pi_1^*$	1.73(0.324)	1.86(0.483)	–
1 $^1B_{3u}$ (x)	$\pi_{-4} \rightarrow \pi_1^*$	2.61(0.029)	2.98(0.050)	–
2 $^1B_{2u}$ (y)	$\pi_{-5} \rightarrow \pi_1^*$	3.17(0.080)	3.57(0.240)	–
2 $^1B_{3u}$ (x)	$\pi_{-3} \rightarrow \pi_2^*$	3.20(0.011)	3.66(0.001)	–
3 $^1B_{2u}$ (y)	$\pi_{-2} \rightarrow \pi_2^*$	3.44(2.022)	3.75(2.186)	–

[a] Absorption in glassy organic solid [18a].
[b] Absorption in *n*-heptane solution [11b].
[c] Absorption in neon-matrix [29e].
[d] Absorption in gas-phase [12j].

Table 6
Same as Table 2 for hexacene in its −1, 0, +1, and +2 charge-states

State (pol.)	Excitation	BLYP	B3LYP	Exp.
Anion (ground-state $^2B_{3g}$)				
1 ^2A_u (x)	$\pi_{-1} \rightarrow \pi_0^*$	0.78(0.006)	0.83(0.011)	–
1 $^2B_{1u}$ (y)	$\pi_0 \rightarrow \pi_1^*$	1.34(0.284)	1.43(0.370)	–
2 ^2A_u (x)	$\pi_{-2} \rightarrow \pi_1^*$	2.41(<0.001)	2.47(<0.001)	–
1 $^2B_{2u}$ (z)	$\pi_0 \rightarrow \pi_3^*$	2.14(<0.001)	2.56(0.001)	–
2 $^2B_{1u}$ (y)	$\pi_{-1} \rightarrow \pi_2^*$	2.51(0.043)	2.71(0.149)	–
Neutral (ground-state ^1A_g)				
1 $^1B_{3u}$ (x,p)	$\pi_{-1} \rightarrow \pi_1^*$	1.24(0.017)	1.51(0.034)	1.90[a]
1 $^1B_{2u}$ (y,α)	$\pi_{-3} \rightarrow \pi_1^*$, $\pi_{-1} \rightarrow \pi_3^*$	2.75(0.009)	3.02(0.010)	2.80[a]
2 $^1B_{3u}$ (x)	$\pi_{-4} \rightarrow \pi_1^*$	2.78(0.001)	3.39(<0.001)	–
3 $^1B_{3u}$ (x)	$\pi_{-1} \rightarrow \pi_4^*$	3.07(0.028)	3.69(0.010)	–
4 $^1B_{3u}$ (x)	$\pi - 2 \rightarrow \pi_2^*$	3.35(0.017)	3.82(0.061)	–
Cation (ground-state ^2A_u)				
1 $^2B_{3g}$ (x)	$\pi_0 \rightarrow \pi_1^*$	0.84(0.006)	0.90(0.010)	–
1 $^2B_{2g}$ (y)	$\pi_{-1} \rightarrow \pi_0^*$	1.27(0.246)	1.34(0.317)	–
2 $^2B_{3g}$ (x)	$\pi_{-3} \rightarrow \pi_1^*$	2.30(<0.001)	2.40(<0.001)	–
2 $^2B_{2g}$ (y)	$\pi_{-2} \rightarrow \pi_1^*$	2.43(0.046)	2.63(0.167)	–
3 $^2B_{3g}$ (x)	$\pi_{-4} \rightarrow \pi_0^*$	2.52(0.007)	2.92(0.021)	–
Dication (ground-state ^1A_g)				
1 $^1B_{2u}$ (y)	$\pi_{-1} \rightarrow \pi_1^*$	1.55(0.440)	1.67(0.652)	–
1 $^1B_{3u}$ (x)	$\pi_{-4} \rightarrow \pi_1^*$	2.43(0.009)	2.83(0.031)	–
2 $^1B_{3u}$ (x)	$\pi_{-3} \rightarrow \pi_2^*$	2.66(0.018)	3.05(0.001)	–
2 $^1B_{2u}$ (y)	$\pi_{-5} \rightarrow \pi_1^*$	2.82(0.062)	3.21(0.130)	–
3 $^1B_{2u}$ (y)	$\pi_{-2} \rightarrow \pi_2^*$	3.10(2.203)	3.44(2.642)	–

[a] Extrapolated from solution spectra to the gas-phase (see compilation in Ref. [26k]).

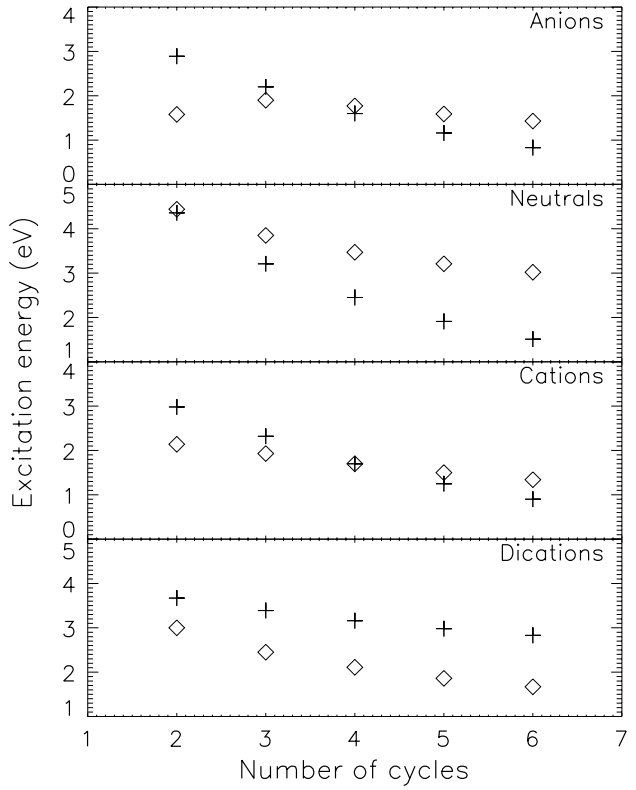

Fig. 9. Calculated positions (B3LYP/6 − 31 + G*) of the lowest short-polarised (crosses, p-bands in the neutral species) and lowest long-polarised (diamonds, α-bands in the neutrals) electronic transitions in the five oligoacenes considered as a function of the size and charge-state of the molecule.

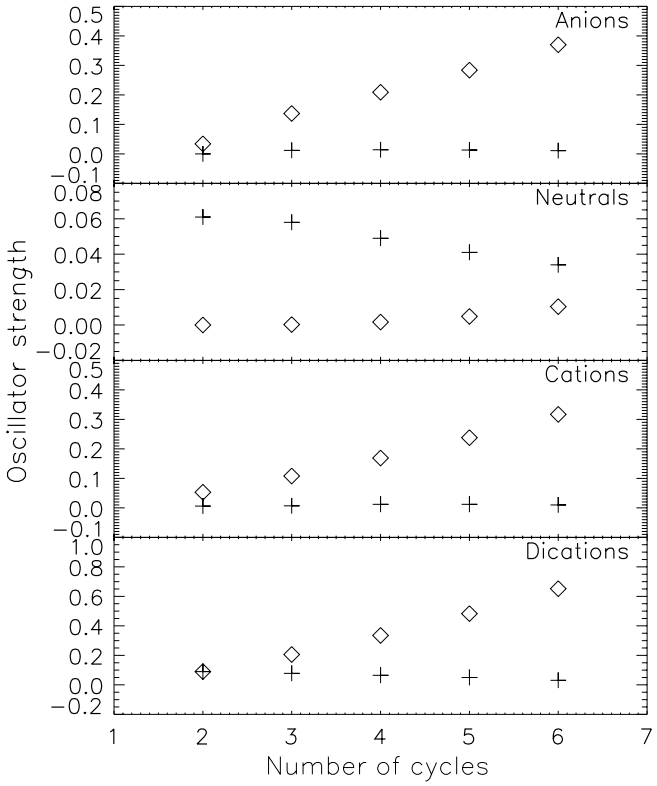

Fig. 10. Same as Fig. 9 for the corresponding oscillator strengths.

tematic decrease with increasing positive charge of the absorption cross-section in the energy gap between the π and σ plasmon-like structures (between ∼6 and ∼12 eV). This same behaviour has been shown for a larger sample of PAHs [23c]. In addition, as expected, the observed scatter between the different charge-states decreases with increasing molecular size.

Concerning the visible–UV part of the spectrum, as reported in Tables 2–6, we checked both the sensitivity of our TD-DFT calculations to the use of different exchange-correlation functionals, and their reliability in comparison with the available experimental data. General agreement is found between BLYP and B3LYP which yield the same ordering of the strongest dipole-allowed excited states. On the average, the BLYP energies are found to be systematically smaller by 0.1–0.6 eV compared to the corresponding B3LYP results, our data confirm the spectral assignment done in previous studies for neutral [26k], and singly charged species [29d,29f]. From the more accurate experimental data reported for the anions, neutrals, and cations we found that the mean relative deviation of the B3LYP functional is of the order of 6%, compared to the mean relative deviation of about 7% given by BLYP. We therefore consider only the former set of results in the following analysis.

The frequency–space implementation of TD-DFT enabled us to gain some insight into the nature of the first few electronic excitations. Focusing only on dications, reported here for the first time, we find that the lowest in-plane long (y) and short-axis (x) polarised bands correspond, respectively, to the HOMO-1 → LUMO ($\pi_{-2} \rightarrow \pi_1^*$) and HOMO-2 → LUMO ($\pi_{-3} \rightarrow \pi_1^*$) transitions for naphthalene and anthracene, and HOMO → LUMO ($\pi_{-1} \rightarrow \pi_1^*$) and HOMO-3 → LUMO ($\pi_{-4} \rightarrow \pi_1^*$) for tetracene, pentacene, and hexacene. Figs. 9 and 10 show interesting trends as to the behaviour of the lowest-lying electronic transitions as a function of the size of the molecule and its charge-state. The positions of both in-plane short and long-polarised excitations are found to shift to lower energies with molecular size for all charge-states considered (Fig. 9). We observe the well-known similarities in the electronic absorption spectra between anionic and cationic PAHs, as well as the systematic shifts in band position when going from the cation to the anion [18a,29f]. The sign and the magnitude of these shifts, attributed to the different effect of the σ-electrons in both ions [18a], are reproduced by TD-DFT for the most intense bands [29f], i.e., the lowest-lying y bands in oligoacenes. For example, the measured blue-shifts of 0.07 eV (from 1.43 eV of the 1^2B_{2g} state of the cation to 1.50 eV of the 1^2B_{1u} state of the anion, data in organic solid [18a], see Table 4) and 0.11 eV (from 1.31 eV of the 1^2A_u state of the cation to 1.42 eV 1^2B_{3g} state of the anion, data in Ne-matrix [29e], see Table 5), when going from the cation to the anion of tetracene and pentacene, respectively, compare favorably with our computed blue-shifts of 0.07, from 1.70 to 1.77 eV, and 0.10 eV, from 1.50 to 1.60 eV (0.05 and

Table 7
Comparison between the B3LYP/6 − 31 + G* results (all values in eV) for the HOMO–LUMO energy gap E_{gap}^{KS} obtained as difference of Kohn–Sham eigenvalues, the excitation energy of the HOMO–LUMO transition as given by TD-DFT, $E_{gap}^{TD\text{-}DFT}$, and its corresponding experimental value E_{gap}^{exp} (p-bands in Tables 2–6)

n	E_{gap}^{KS}	$E_{gap}^{TD\text{-}DFT}$	E_{gap}^{exp}	QP_{gap}^{1}	QP_{gap}^{2}	$QP_{gap}^{DFT\text{-}GW}$	QP_{gap}^{exp}	E_{bind}	E_{bind}^{exp}
2	4.74(4.75)	4.36(4.35)	4.45	8.27(8.29)	8.12	8.0	8.34	3.91	3.89
3	3.54(3.55)	3.21(3.21)	3.45	6.66(6.60)	6.58	6.6	6.91	3.45	3.46
4	2.74(2.75)	2.45(2.44)	2.72	5.55(5.56)	5.50	5.5	5.90	3.10	3.18
5	2.19(2.19)	1.91(1.90)	2.31	4.75(4.76)	4.72	4.8	5.20	2.84	2.89
6	1.78(1.78)	1.51(1.50)	1.90	4.15(4.16)	4.13	4.3	–	2.64	–

The QP–gap evaluated using Eqs. (1) and (2) is compared with the DFT-based tight-binding GW data of Ref. [28d], QP_{gap}^{DFT-GW}, as well as with the experimental value QP_{gap}^{exp} obtained as the difference between the experimental EAs and first IEs given in Table 1. The theoretical and experimental exciton binding energy E_{bind} are estimated as $QP_{gap}^{1} - E_{gap}^{TD-DFT}$ and $QP_{gap}^{exp} - E_{gap}^{exp}$, respectively. For comparison, the results of Ref. [26k] are reported within parentheses.

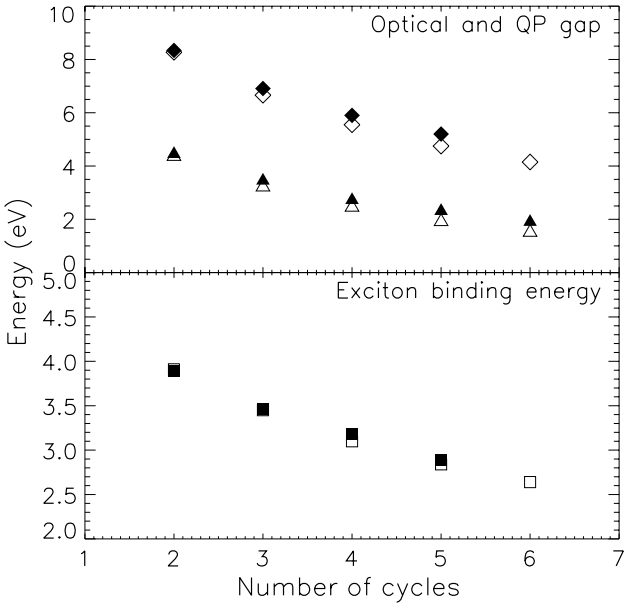

Fig. 11. Top panel: optical gap $E_{gap}^{TD\text{-}DFT}$ as obtained via TD-DFT at the B3LYP/6 − 31 + G* level (open triangles) and ΔSCF QP-corrected HOMO–LUMO gap QP_{gap}^{1} computed via Eq. (1) (open diamonds), as a function of molecular size. Bottom panel: exciton binding energy E_{bind} estimated as $QP_{gap}^{1} - E_{gap}^{TD\text{-}DFT}$ (open squares). In both figures, the corresponding experimental values are represented by the filled symbols (see Table 7).

0.08 in Ref. [29f]). However, this is not the case for the lowest-lying x bands, for which our theoretical predictions seem to present a mismatch. In the case of tetracene and pentacene, e.g., the experimental blue-shifts of 0.04 eV (from 1.66 eV of the 1^2B_{3g} state to 1.7 eV of the 1^2A_u state, Table 4), and 0.10 eV (from 1.27 eV of the 1^2B_{1u} state to 1.37 eV of the 1^2B_{2g} state, Table 5), are predicted in this study to be red-shifted by −0.10, from 1.70 to 1.60 eV, and −0.09 eV, from 1.25 to 1.16 eV, respectively (−0.06 and −0.05 in Ref. [29f]).

We confirm the system-size-dependent errors found for the short-polarised transitions (p bands) in the neutral systems [26g,26k]. More specifically, from a comparison with the available experimental data reported in Tables 2–6 we find that while the relative error in the position of the α band is always of the order of 10%, in the case of the p band this error increases from 2% for naphthalene to 20% for hexacene (see the triangles on the top panel of Fig. 11). On the other hand, we find the position of the β band to be reproduced with a good precision with relative errors of, at most, 4%. In the case of the radical anions and cations, we could not find clear trends as to the performances of our TD-DFT/B3LYP results. On the average, the relative errors are larger for the long-polarised bands compared to the short-polarised ones for both anions (12% vs. 9%) and cations (16% vs. 7%).

The oscillator strengths f we obtain for the oligoacenes are also found to display systematic changes as a function of molecular size (Fig. 10). Unlike the neutral molecules, in all charged species the lowest parallel (y) transitions have larger f-values compared to the corresponding lowest perpendicular (x) ones. The oscillator strengths of the x-polarised transitions display small changes with the number of benzene units being always of the order of 0.01 for cations and anions, and decreasing from 0.06 to 0.03 and from 0.09 to 0.03 for neutrals and dications, respectively. The oscillator strengths obtained for the y-polarised transitions are found to increase with the molecular size for all the charge-states considered. In particular, while the increase for the neutral molecules is from 1×10^{-5} to 1×10^{-2} when going from naphthalene to hexacene, for the charge-states −1, +1, and +2 the corresponding values go from 0.03 to 0.37, 0.05 to 0.32, and from 0.09 to 0.65. Therefore, analogously to singly charged species, doubly ionised PAHs have strong absorption features in the near-IR, visible, and near-UV spectral ranges, a result that might be relevant in the astrophysical context.

Orbital energy differences are well-defined zeroth-order approximations to electronic excitation energies [33j]. As shown in Table 7, the HOMO–LUMO energy gap obtained directly as difference of Kohn–Sham eigenvalues gives a better description of the optical gap, i.e., the position of the p-band, with relative errors in the range 1–6%, compared to TD-DFT. As already discussed, in this latter case a system-size-dependent error is known to exist [26g], with an increase from 2% to 20% in the relative error as found in this study when going from naphthalene to

hexacene. The ΔSCF QP-corrected HOMO–LUMO gaps of neutral oligoacenes as computed at the B3LYP/$6-31+G^*$ level, compare very well with the DFT-based tight-binding GW calculated ones independently from the size of the system, with discrepancies no larger than 3%. These values, however, when compared to experiments appear to be affected by the same systematic error found for the TD-DFT results (see the diamonds on the top panel of Fig. 11). On the other hand, since these errors cancel each other in the evaluation of the exciton binding energy, we obtain an accurate estimate for E_{bind}. Appreciable excitonic effects due to both quantum confinement and reduction of screening are found, with values ranging from 3.9 eV for naphthalene to 2.8 eV for hexacene.

5. Concluding remarks

We presented a systematic theoretical study of the five smallest oligoacenes, i.e., naphthalene, anthracene, tetracene, pentacene, and hexacene in the charge-states most relevant for astrophysical applications, namely −1, 0, +1, and +2. From the ground-state structural relaxations performed at the B3LYP/$6-31+G^*$ level we computed the electron affinities, the first and second ionisation energies, the quasiparticle correction to the HOMO–LUMO gap of the neutral systems, and an estimate of the excitonic effects in this class of compounds. Good agreement is found with the available experimental data as well as with previous theoretical results. To study the electronic absorption spectra we used a compendium of the TD-DFT theoretical framework in both real-time, to obtain the whole photo-absorption cross-sections in a single step, and frequency space, to study general trends as a function of charge-state and molecular size for the lowest-lying valence $\pi \rightarrow \pi^*$ in-plane long-polarised and short-polarised electronic transitions. The main step forward achieved in this work with respect to previous theoretical analyses lies (i) in the spectral range covered, that extends up to the far-UV for both neutral and charged PAHs, and (ii) in the first detailed study of doubly ionised species, largely unexplored so far. The interest on PAH dications by the astrophysical community has been recently renewed by the proposal that they could be plausible candidates to explain a red fluorescence observed in many interstellar sources [32]. We find that dications, like their singly charged counterparts, display strong electronic transitions of $\pi \rightarrow \pi^*$ character in the near-IR, visible, and near-UV spectral ranges. As expected, the broad plasmon-like structure peaking at about 17.5 eV is found to be relatively insensitive to the charge-state of the molecule, but we interestingly find a systematic decrease with increasing positive charge of the absorption cross-section between about 6 eV and about 12 eV. Since the latter spectral signature is a general property of all PAHs [23c], a comparison with astronomical extinction curves could provide an additional observational handle for estimating the average charge-state of interstellar PAHs.

Acknowledgements

G. Malloci acknowledges financial support by Regione Autonoma della Sardegna. G.C., G.M., and G.M. acknowledge financial support by MIUR under project PON-CyberSar. We thank the authors of OCTOPUS for making their code available under a free license. We acknowledge the High Performance Computational Chemistry Group for the use of NWCHEM, A Computational Chemistry Package for Parallel Computers, Version 4.7 (2005), PNNL, Richland, Washington, USA. Part of the simulations were carried out at CINECA (Bologna).

Appendix A. Supplementary data

Supplementary data associated with this article can be found, in the online version, at doi:10.1016/j.chemphys.2007.07.046.

References

[1] (a) E. Clar, Aromatische Kohlenwasserstoffe, Springer, Berlin, 1941; (b) E. Clar Polycyclic Hydrocarbons, Vols. 1 and 2, Academic Press, London, 1964.
[2] (a) R.F. Curl, Nature 363 (1993) 14; (b) C.J. Pope, J.A. Marr, J.B. Howard, J. Phys. Chem. 97 (1993) 11001.
[3] (a) R.G. Harvey, Polycyclic Aromatic Hydrocarbons: Chemistry and Carcinogenesis, Cambridge University Press, Cambridge, 1991; (b) M. Rehwagen, A. Müller, L. Massolo, O. Herbarth, A. Ronco, Sci. Total Environ. 348 (2005) 199.
[4] (a) J.H. Hahn, R. Zenobi, J.L. Bada, R.N. Zare, Science 239 (1988) 1523; (b) S.J. Clemett, C.R. Maechling, R.N. Zare, P.D. Swan, R.M. Walker, Science 262 (1993) 721; (c) A.G.G.M. Tielens, The Physics and Chemistry of the Interstellar Medium, Cambridge University Press, Cambridge, 2005.
[5] (a) M. Bendikov, F. Wudl, D.F. Perepichka, Chem. Rev. 104 (2004) 4891; (b) K. Hummer, P. Puschnig, C. Ambrosch-Draxl, Phys. Rev. Lett. 92 (2004) 147402-1; (c) K. Hummer, C. Ambrosch-Draxl, Phys. Rev. B 71 (2005) 081202-1; (d) K. Hummer, C. Ambrosch-Draxl, Phys. Rev. B 72 (2005) 205205-1.
[6] (a) S.F. Nelson, Y.Y. Lin, D.J. Gundlach, T.N. Jackson, Appl. Phys. Lett. 72 (1998) 1854; (b) H. Klauk, M. Halik, U. Zschieschang, G. Schmid, W. Radlik, J. Appl. Phys. 92 (2002) 5259.
[7] (a) H. Aziz, Z.D. Popovic, Appl. Phys. Lett. 80 (2002) 2180; (b) Y. Kan, L. Wang, H. Yunchuan, W. Guoshi, Q. Yong, Appl. Phys. Lett. 84 (2004) 1513.
[8] (a) G.K.R. Senadeera, P.V.V. Jayaweera, V.P.S. Perera, K. Tennakone, Sol. Energy Mater. Sol. Cells 73 (2002) 103; (b) S. Yoo, B. Domercq, B. Kippelen, Appl. Phys. Lett. 85 (2004) 5427.
[9] I. Shiyanovkaya, K.D. Singer, V. Percec, T.K. Bera, Y. Miura, M. Glodde, Phys. Rev. B 67 (2003) 035204.
[10] (a) J.E. Anthony, Chem. Rev. 106 (2006) 5028; (b) M. Winkler, K.N. Houk, J. Am. Chem. Soc. 129 (2007) 1805.
[11] (a) J.R. Platt, J. Chem. Phys. 17 (1949) 484; (b) H.B. Klevens, J.R. Platt, J. Chem. Phys. 17 (1949) 470.
[12] (a) A. Bree, L.E. Lyons, J. Chem. Soc. (1960) 5206; (b) L.E. Lyons, G.C. Morris, J. Mol. Spectrosc. 4 (1960) 480;

(c) G.A. George, G.C. Morris, J. Mol. Spectrosc. 26 (1968) 67;
(d) A. Bergman, J. Jortner, Chem. Phys. Lett. 15 (1972) 309;
(e) E.E. Koch, A. Otto, Chem. Phys. Lett. 12 (1972) 476;
(f) E.E. Koch, A. Otto, K. Radler, Chem. Phys. Lett. 16 (1972) 131;
(g) E.E. Koch, A. Otto, K. Radler, Chem. Phys. Lett. 21 (1973) 501;
(h) C. Joblin, Ph.D. Thesis, Université Paris 7, 1992.;
(i) C. Joblin, A. Léger, P. Martin, Astrophys. J. 393 (1992) L79;
(j) E. Heinecke, D. Hartmann, R. Müller, A. Hese, J. Chem. Phys. 109 (1998) 906.

[13] (a) E.E. Koch, A. Otto, Opt. Commun. 1 (1969) 47;
(b) R.H. Hubner, S.R. Mielczarek, C.E. Kuyatt, Chem. Phys. Lett. 16 (1972) 464;
(c) M.A. Khakoo, J.M. Ratliff, S. Trajmar, J. Chem. Phys. 93 (1990) 8816;
(d) J.W. Keller, M.A. Colan, R. Goruganthu, Astrophys. J. 391 (1992) 872.

[14] (a) I.B. Berlman, Handbook of Fluorescence Spectra of Aromatic Molecules, Academic Press, New York, 1971;
(b) W.R. Lambert, P.M. Felker, J.A. Syage, A.H. Zewail, J. Chem. Phys. 81 (1984) 2195;
(c) M.S. Gudipati, J. Daverkausen, G. Hohlneicher, Chem. Phys. 173 (1993) 143;
(d) F. Ossler, T. Metz, M. Aldén, Appl. Phys. B 72 (2001) 465;
(e) F. Ossler, T. Metz, M. Aldén, Appl. Phys. B 72 (2001) 479;
(f) C. Reylé, P. Bréchignac, Eur. Phys. J. D 8 (2000) 205.

[15] (a) F. Mason, R.D. Peacock, Chem. Phys. Lett. 21 (1973) 406;
(b) E. Sackmann, H. Möhwald, J. Chem. Phys. 58 (1973) 5407;
(c) R.P. Steiner, J. Michl, J. Am. Chem. Soc. 100 (1978) 6861.

[16] (a) R. Boschi, E. Clar, W. Schmidt, J. Chem. Phys. 60 (1974) 4406;
(b) W. Schmidt, J. Chem. Phys. 66 (1977) 828;
(c) M.C.R. Cockett, H. Ozeki, K. Okuyama, K. Kimura, J. Chem. Phys. 98 (1993) 7763;
(d) J. Schiedt, R. Weinkauf, Chem. Phys. Lett. 266 (1997) 201;
(e) J. Schiedt, W.J. Knott, K. Le Barbu, E.W. Schlag, R. Weinkauf, J. Chem. Phys. 113 (2000) 9470;
(f) N.E. Gruhn, D.A. da Silva Filho, T.G. Bill, M. Malagoli, V. Coropceanu, A. Kahn, J.-L. Bredas, J. Am. Chem. Soc. 124 (2002) 7918.

[17] (a) J.W. Hager, S.C. Wallace, Anal. Chem. 60 (1988) 5;
(b) H.W. Jochims, H. Baumgärtel, S. Leach, Astron. Astrophys. 314 (1996) 1003;
(c) Y. Ling, C. Lifshitz, Chem. Phys. Lett. 257 (1996) 587;
(d) H.W. Jochims, E. Rühl, H. Baumgärtel, S. Tobita, S. Leach, Int. J. Mass. Spectr. Ion Proc. 167/168 (1997) 35.

[18] (a) T. Shida, S. Iwata, J. Am. Chem. Soc. 95 (1973) 3473;
(b) T. Shida, Electronic Absorption Spectra of Radical Ions, Elsevier, Amsterdam, 1988.

[19] (a) L. Andrews, T.A. Blankenship, J. Am. Chem. Soc. 103 (1981) 5977;
(b) B.J. Kelsall, L. Andrews, J. Chem. Phys. 76 (1982) 5005;
(c) L. Andrews, R.S. Friedmann, B.J. Kelsall, J. Phys. Chem. 89 (1985) 4016;
(d) F. Salama, L.J. Allamandola, J. Chem. Phys. 94 (1991) 6964;
(e) J. Szczepanski, M. Vala, D. Talbi, O. Parisel, Y. Ellinger, J. Chem. Phys. 98 (1993) 4494;
(f) F. Salama, C. Joblin, L.J. Allamandola, J. Chem. Phys. 101 (1992) 10252;
(g) J. Szczepanski, J. Drawdy, C. Walburg, M. Vala, Chem. Phys. Lett. 245 (1995) 539;
(h) C. Joblin, F. Salama, L. Allamandola, J. Chem. Phys. 102 (1995) 9743;
(i) C. Joblin, F. Salama, L. Allamandola, J. Chem. Phys. 110 (1999) 7287;
(j) X. Chillier, P. Boulet, H. Chermette, F. Salama, J. Weber, J. Chem. Phys. 115 (2001) 1769;
(k) X.D.F. Chillier, B.M. Stone, C. Joblin, F. Salama, L.J. Allamandola, J. Chem. Phys. 116 (2002) 5725.

[20] (a) P. Bréchignac, T. Pino, Astron. Astrophys. 343 (1999) L49;
(b) T. Pino, N. Boudin, P. Bréchignac, J. Chem. Phys. 111 (1999) 7337;
(c) P. Bréchignac, T. Pino, N. Boudin, Spectrochim. Acta A 57 (2001) 745.

[21] (a) M. Hartmann, A. Lidinger, J.P. Toennies, A.F. Vilesov, J. Phys. Chem. A 105 (2001) 6369;
(b) M. Hartmann, A. Lidinger, J.P. Toennies, A.F. Vilesov, Phys. Chem. Chem. Phys. 4 (2002) 4839;
(c) G. Rouillé, S. Krasnokutski, F. Huisken, T. Henning, O. Sukhorukov, A. Staicu, J. Chem. Phys. 120 (2004) 6028;
(d) S. Krasnokutski, G. Rouillé, F. Huisken, Chem. Phys. Lett. 406 (2005) 386.

[22] (a) D. Romanini, L. Biennier, F. Salama, A. Kachanov, L.J. Allamandola, F. Stoeckel, Chem. Phys. Lett. 303 (1999) 165;
(b) L. Biennier, F. Salama, L.J. Allamandola, J.J. Scherer, J. Chem. Phys. 118 (2003) 7863;
(c) L. Biennier, F. Salama, M. Gupta, A. O'Keefe, Chem. Phys. Lett. 387 (2004) 287;
(d) O. Sukhorukov, A. Staicu, E. Diegel, G. Rouillé, T. Henning, F. Huisken, Chem. Phys. Lett. 386 (2004) 259;
(e) X. Tan, F. Salama, J. Chem. Phys. 122 (2005) 084318;
(f) X. Tan, F. Salama, J. Chem. Phys. 123 (2005) 014312;
(g) A. Staicu, S. Krasnokutski, G. Rouillé, T. Henning, F. Huisken, J. Mol. Struct. 786 (2006) 105.

[23] (a) G. Malloci, G. Mulas, C. Joblin, Astron. Astrophys. 426 (2004) 105;
(b) G. Malloci, G. Mulas, G. Cappellini, V. Fiorentini, I. Porceddu, Astron. Astrophys. 432 (2005) 585;
(c) G. Malloci, C. Joblin, G. Mulas, Astron. Astrophys. 462 (2007) 627;
(d) G. Malloci, C. Joblin, G. Mulas, Chem. Phys. 332 (2007) 353;
(e) M.A.L. Marques, A. Castro, G. Malloci, G. Mulas, S. Botti, J. Chem. Phys. 127 (2007) 014107-1.

[24] (a) G. Mulas, G. Malloci, C. Joblin, D. Toublanc, Astron. Astrophys. 446 (2006) 537;
(b) G. Mulas, G. Malloci, C. Joblin, D. Toublanc, Astron. Astrophys. 456 (2006) 161;
(c) G. Mulas, G. Malloci, C. Joblin, D. Toublanc, Astron. Astrophys. 460 (2006) 93.

[25] (a) R.C. Peck, J.M. Schulman, R.L. Disch, J. Phys. Chem. 94 (1990) 6637;
(b) D.J. De Frees, M.D. Miller, D. Talbi, F. Pauzat, Y. Ellinger, Astrophys. J. 408 (1993) 530;
(c) J. Cioslowski, G. Liu, M. Martinov, P. Piskorz, D. Moncrieff, J. Am. Chem. Soc. 118 (1996) 5261.

[26] (a) K.B. Wiberg, J. Org. Chem. 62 (1997) 5720;
(b) H.H. Heinze, A. Görling, N. Rösch, J. Chem. Phys. 113 (2000) 2088;
(c) M.S. Deleuze, A.B. Trofimov, L.S. Cederbaum, J. Chem. Phys. 115 (2004) 5859;
(d) K.A. Nguyen, J. Kennel, R. Pacther, J. Chem. Phys. 117 (2002) 7128;
(e) M.S. Deleuze, L. Claes, E.S. Kryachko, J.-P. François, J. Chem. Phys. 119 (2003) 3106;
(f) M. Parac, S. Grimme, Chem. Phys. 292 (2003) 11;
(g) S. Grimme, M. Parac, Chem. Phys. Chem. 3 (2003) 292;
(h) M. Dierksen, S. Grimme, J. Chem. Phys. 120 (2004) 3544;
(i) M. Dierksen, S. Grimme, J. Phys. Chem. A 108 (2004) 10225;
(j) W.–Q. Deng, W.A. Goddard III, J. Phys. Chem. B 108 (2004) 8614;
(k) E.S. Kadantsev, M.J. Stott, A. Rubio, J. Chem. Phys. 124 (2006) 134901-1.

[27] (a) T. Hashimoto, H. Nakano, K. Hirao, J. Chem. Phys. 104 (1996) 6244;
(b) Y. Kawashima, T. Hashimoto, H. Nakano, K. Hirao, Theor. Chem. Acc. 102 (1999) 49.

[28] (a) R. Notario, J.M. Abboud, J. Phys. Chem. A 102 (1998) 5290;
(b) K.N. Houk, P.S. Lee, M. Nendel, J. Org. Chem. 66 (2001) 5517;
(c) M. Bendikov, H.M. Duong, K. Starkey, K.N. Houk, E.A. Carter, F. Wudl, J. Am. Chem. Soc. 126 (2004) 7416;
(d) T.A. Niehaus, M. Rohlfing, F. della Sala, A. di Carlo, T. Frauenheim, Phys. Rev. A 71 (2005) 022508-1.
[29] (a) F. Negri, M.Z. Zgierski, J. Phys. Chem. 100 (1994) 2819;
(b) C. Niederalt, S. Grimme, S.D. Peyerimhoff, Chem. Phys. Lett. 245 (1995) 455;
(c) T. Bally, C. Carra, M.P. Fülscher, Z. Zhu, J. Chem. Soc. Perkin Trans. 2 (1998) 1759;
(d) S. Hirata, T.J. Lee, M. Head-Gordon, J. Chem. Phys. 111 (1999) 8904;
(e) T.M. Halasinski, D.M. Hudgins, F. Salama, L.J. Allamandola, T. Bally, J. Phys. Chem. A 104 (2000) 7484;
(f) S. Hirata, M. Head-Gordon, J. Szczepanski, M. Vala, J. Phys. Chem. A 107 (2003) 4940;
(g) F. Jolibois, A. Klotz, F.X. Gadéa, C. Joblin, Astron. Astrophys. 444 (2005) 629;
(h) T. Pino, P. Parneix, F. Calvo, P. Bréchignac, J. Phys. Chem. A 111 (2007) 4456.
[30] (a) C.E.H. Dessent, Chem. Phys. Lett. 330 (2000) 180;
(b) C.W. Bauschlicher, Chem. Phys. Lett. 409 (2005) 235.
[31] (a) S. Leach, J. Electr. Spectr. Rel. Phen. 41 (1986) 427;
(b) S. Leach, Planet. Space Sci. 43 (1995) 1153;
(c) S. Tobita, S. Leach, H.W. Jochins, E. Rühl, E. Illenberger, H. Baumgärtel, Can. J. Phys. 72 (1994) 1060.
[32] A.N. Witt, K.D. Gordon, U.P. Vijh, P.H. Sell, T.L. Smith, R.-H. Xie, Astrophys. J. 636 (2006) 303.
[33] (a) P. Hohenberg, W. Kohn, Phys. Rev. 136 (1964) B864;
(b) W. Kohn, L.J. Sham, Phys. Rev. 140 (1965) A1133;
(c) J.P. Perdew, A. Zunger, Phys. Rev. B 23 (1981) 5048;
(d) A.D. Becke, Phys. Rev. A 38 (1988) 3098;
(e) C. Lee, W. Yang, R. Parr, Phys. Rev. B 37 (1988) 785;
(f) R.W. Godby, M. Schlüter, L.J. Sham, Phys. Rev. B 37 (1988) 10159;
(g) R.O. Jones, O. Gunnarsson, Rev. Mod. Phys. 61 (1989) 689;
(h) R.M. Dreizler, E.K.U. Gross, Density Functional Theory, Springer, Berlin, 1990;
(i) A.D. Becke, J. Chem. Phys. 98 (1993) 5648;
(j) A. Görling, Phys. Rev. A 54 (1996) 3912;
(k) E.J. Baerends, O.V. Gritsenko, J. Phys. Chem. A 101 (1997) 5383.
[34] (a) E. Runge, E.K.U. Gross, Phys. Rev. Lett. 52 (1984) 997;
(b) M.E. Casida, in: D.P. Chong (Ed.), Recent Advances in Density Functional Theory, Vol. I, World Scientific, Singapore, 1995;
(c) R. Bauernschmitt, R. Ahlrichs, Chem. Phys. Lett. 256 (1996) 454;
(d) K.B. Wiberg, R.E. Stratmann, M.J. Frish, Chem. Phys. Lett. 297 (1998) 60;
(e) S. Hirata, M. Head-Gordon, Chem. Phys. Lett. 302 (1999) 375;
(f) S. Hirata, M. Head-Gordon, Chem. Phys. Lett. 314 (1999) 291;
(g) K. Yabana, G.F. Bertsch, Int. J. Quant. Chem. 75 (1999) 55;
(h) M.E. Casida, D. Salahub, J. Chem. Phys. 113 (2000) 8918;
(i) M.A.L. Marques, E.K.U. Gross, Ann. Rev. Phys. Chem. 55 (2004) 3425;
(j) A. Dreuw, M. Head-Gordon, Chem. Rev. 105 (2005) 4009;
(k) K. Burke, J. Werschnick, E.K.U. Gross, J. Chem. Phys. 123 (2005) 062206.
[35] (a) J.M.L. Martin, J. El-Yazal, J. Francois, J. Phys. Chem. 100 (1996) 15358;
(b) S.R. Langhoff, J. Phys. Chem 100 (1996) 2819;
(c) C.W. Bauschlicher, S.R. Langhoff, Spectr. Acta A 53 (1997) 1225;
(d) T. Kato, K. Yoshizawa, T. Yamabe, J. Chem. Phys. 110 (1999) 249;
(e) T. Kato, T. Yamabe, Curr. Appl. Phys. 1 (2001) 295;
(f) D. Schröder, J. Loos, H. Schwarz, R. Thissen, D.V. Preda, L.T. Scott, D. Caraiman, M.V. Frach, D.K. Böhme, Helv. Chim. Acta 84 (2001) 1625;
(g) J.C. Rienstra-Kiracofe, C.J. Barden, S.T. Brown, H.F. Schaefer III, J. Phys. Chem. A 105 (2001) 524;
(h) T. Kato, K. Yoshizawa, K. Hirao, J. Chem. Phys. 116 (2002) 3420;
(i) T. Kato, T. Yamabe, J. Chem. Phys. 117 (2002) 2324;
(j) T. Kato, T. Yamabe, Chem. Phys. Lett. 403 (2005) 113;
(k) A. Modelli, L. Mussoni, D. Fabbri, J. Phys. Chem. A 110 (2006) 6482.
[36] (a) M.E. Casida, C. Jamorski, K.C. Casida, D. Salahub, J. Chem. Phys. 108 (1998) 4439;
(b) D.J. Tozer, N.C. Handy, J. Chem. Phys. 109 (1998) 10180;
(c) N.C. Handy, D.J. Tozer, J. Comput. Chem. 20 (1999) 106.
[37] (a) R.J. Cave, F. Zhang, N.T. Maitra, K. Burke, Chem. Phys. Lett. 389 (2004) 39;
(b) N.T. Maitra, F. Zhang, R.J. Cave, K. Burke, J. Chem. Phys. 120 (2004) 5932.
[38] (a) D.J. Tozer, R.D. Amos, N.C. Handy, B.O. Roos, L. Serrano-Andres, Mol. Phys. 97 (1999) 859;
(b) A.L. Sobolewski, W. Domcke, Chem. Phys. 294 (2003) 73;
(c) A. Dreuw, M. Head-Gordon, J. Am. Chem. Soc. 126 (2004) 4007.
[39] Z.-L. Cai, K. Sendt, J.R. Reimers, J. Chem. Phys. 117 (2002) 5543.
[40] (a) T.M. Halasinski, J.L. Weisman, R. Ruiterkamp, T.J. Lee, F. Salama, M. Head-Gordon, J. Phys. Chem. A 107 (2003) 3660;
(b) J.L. Weisman, T.J. Lee, F. Salama, M. Head-Gordon, Astrophys. J. 587 (2003) 256;
(c) J.L. Weisman, A. Mattioda, T.J. Lee, D. Hudgins, L.J. Allamandola, C.W. Bauschlicher, M. Head-Gordon, Phys. Chem. Chem. Phys. 7 (2005) 109.
[41] P.J. Sarre, J. Mol. Spectr. 238 (2006) 1.
[42] T.P. Straatsma et al., NWChem, a computational chemistry package for parallel computers, version 4.7, 2005.
[43] (a) J. Gauss, J.F. Stanton, J. Phys. Chem. A 104 (2000) 2865;
(b) G.I. Nemeth, H.L. Selzle, E.W. Schlag, Chem. Phys. Lett. 215 (1993) 151;
(c) P.D. Burrow, J.A. Michejda, K.D. Jordan, J. Chem. Phys. 86 (1987) 9;
(d) L.W. Pickett, M. Muntz, E.M. McPherson, J. Am. Chem. Soc. 73 (1951) 4862.
[44] (a) L. Hedin, Phys. Rev. 139 (1965) A796;
(b) M.S. Hybertsen, S.G. Louie, Phys. Rev. B 34 (1986) 5390.
[45] (a) M.A.L. Marques, A. Castro, A. Rubio, J. Chem. Phys. 115 (2001) 3006;
(b) A. Castro, M.A.L. Marques, J.A. Alonso, G.F. Bertsch, K. Yabana, A. Rubio, J. Chem. Phys. 116 (2002) 1930;
(c) M.A.L. Marques, A. Castro, G.F. Bertsch, A. Rubio, Comp. Phys. Commun. 151 (2003) 60;
(d) X. Lopez, M.A.L. Marques, A. Castro, A. Rubio, J. Am. Chem. Soc. 127 (2005) 12329.
[46] (a) D.M. Ceperley, B.J. Alder, Phys. Rev. Lett. 45 (1980) 566;
(b) N. Troullier, J.L. Martins, Phys. Rev. B 43 (1991) 1993.
[47] S. Lias, in: P.J. Linstrom, W.G. Mallard (Eds.), NIST Chemistry WebBook, NIST Standard Reference Database Number 69. <http://webbook.nist.gov>, Gaithersburg MD, 2005.
[48] L. Crocker, T.B. Wang, P. Kebarle, J. Am. Chem. Soc. 115 (1993) 7818.